Article:
Liu, Z, Gromov, A and Papić, Z orcid.org/0000-0002-8451-2235 (2018) Geometric quench and nonequilibrium dynamics of fractional quantum Hall states. Physical Review B, 98 (15). 155140. ISSN 2469-9950

https://doi.org/10.1103/PhysRevB.98.155140

Geometric quench and non-equilibrium dynamics of fractional quantum Hall states

Zhao Liu,[1] Andrey Gromov,[2] and Zlatko Papić[3]

[1] *Freie Universität Berlin, Dahlem Center for Complex Quantum Systems and Institut für Theoretische Physik, Arnimallee 14, 14195 Berlin, Germany*
[2] *Kadanoff Center for Theoretical Physics, University of Chicago, Illinois 60637, USA*
[3] *School of Physics and Astronomy, University of Leeds, Leeds LS2 9JT, UK*

(Dated: May 31, 2018)

We introduce a quench of the geometry of Landau level orbitals as a probe of non-equilibrium dynamics of fractional quantum Hall (FQH) states. We show that such geometric quenches induce coherent many-body dynamics of neutral degrees of freedom of FQH fluids. The simplest case of mass anisotropy quench can be experimentally implemented as a sudden tilt of the magnetic field, and the resulting dynamics reduces to the harmonic motion of the spin-2 "graviton" mode, i.e., the long wavelength limit of the Girvin-MacDonald-Platzman magnetoroton. We derive analytical description of the graviton dynamics using the bimetric theory of FQH states, and find agreement with exact numerical simulations at short times. We show that certain types of geometric quenches excite higher-spin collective modes, thus establishing their existence in a microscopic model and motivating an extension of geometric theories of FQH states.

PACS numbers: 73.43.Lp, 71.10.Pm

I. INTRODUCTION

Fractional quantum Hall (FQH) states are an epitome of topological phases of matter, featuring exotic phenomena such as fractionalization [1], topological order [2], and protected edge excitations [3, 4]. These phenomena arise as emergent properties of a two-dimensional (2D) electron system in a perpendicular magnetic field [5]. As a consequence of Landau level quantization, electrons in these systems have negligible kinetic energy, which paves the way for Coulomb interaction to produce a variety of exotic effects, whose experimental hallmark is the fractional quantization of the Hall conductance [6].

Given the intricate, purely interacting nature of FQH states, it comes as no surprise that the existing research mainly focused on their equilibrium (static) properties at zero temperature. These properties have often been described using two closely related frameworks: trial wave functions [1, 7–9] and topological quantum field theory (TQFT) [10], which encode the linear response functions [11, 12], exotic quasiparticles ("anyons") [13, 14] characterized by the fractional charge, spin and statistics [15], robust edge modes [4] and the topological degeneracy on a torus [2, 16]. The predictions of microscopic trial states and TQFT have been tested in numerical simulations of unprecedented accuracy, in particular in the case of Laughlin [1, 17] and composite fermion states [18].

Besides the low-energy properties, the complete understanding of a quantum system requires the understanding of its *dynamics*, which is determined by the system's excited states (possibly at non-zero energy density). This dynamics can be physically probed using the global quantum quench: prepare the system in its ground state $|\psi_0\rangle$; abruptly change the Hamiltonian, $H \to H'$; let the system evolve and perform measurements on the time-evolved state. For systems which are intrinsically decoupled from the environment, this quench amounts to the innocuous-looking Schrödinger evolution, $|\psi(t)\rangle = \exp(-iH't)|\psi_0\rangle$, where $|\psi_0\rangle$, crucially, is *not* an eigenstate of the quench Hamiltonian, H'. Even though the Schrödinger evolution can be written in such a compact way, it can nevertheless produce incredibly complex outcomes as it might involve highly excited eigenstates of H'. In one-dimensional integrable systems, where such eigenstates can be computed using techniques like algebraic Bethe ansatz, a particularly deep theoretical understanding of quenches has been achieved (see the recent review [19]) and verified in cold atom experiments [20]. Other notable examples include one-dimensional critical systems where conformal invariance allows to analytically describe the post-quench dynamics of various observables (see Ref. [21] and references therein) and their holographic duals [22], where quantum quench is interpreted as a process of black hole formation and decay.

In this work we introduce a new type of *geometric quench* to study dynamics of FQH states out of equilibrium. While in integrable systems the term "geometric quench" refers to a sudden change of the size of system [23–26] (e.g., controlled by the trap potential in cold atomic systems), our setup assumes that the size of the system remains fixed, but the geometry of Landau level orbitals undergoes an abrupt change. This way of probing the system is quite physical: changing the geometry of Landau level orbitals can be achieved directly by tilting the magnetic field, i.e., by introducing a component of magnetic field tangential to the plane occupied by the particles. Tilted field technique is regularly employed in FQH experiments to measure spin polarization of various states [27], while more recently it has also been used to map out the anisotropy of the composite fermion Fermi surface [28].

Geometric quench is designed to excite the neutral degrees of freedom of FQH states, which have certain universal features that are geometric in nature. Two major

examples are the geometric response function known as Hall viscosity [29–31] and the geometric degrees of freedom responsible for the nematic transition [32, 33]. The former can be understood in terms of response to the variations of ambient geometry [12, 34–41], while the latter can be formulated as fluctuating geometry [42, 43] (see also Ref. [44] for a related perspective). We will show that the real-time dynamics following the geometric quench is accurately described by the excitations of geometric degrees of freedom that characterize the underlying FQH states [42].

More specifically, in the case of Laughlin states, we will show that a (weak) geometric quench driven by an abrupt change of the effective mass tensor of particles excites a single degree of freedom that carries angular momentum (or spin) $L = 2$, which can be viewed as a fluctuating, "intrinsic metric" [45]. This spin-2 degree of freedom is described by a symmetric matrix, which makes it formally similar to the fluctuating space-time metric — a variable that one would like to use in a theory of quantum gravity. For the lack of a better term we will continue to refer to this geometric degree of freedom as "graviton" [46, 47]. The geometric quench thus allows to excite the emergent FQH graviton and to observe its non-trivial dynamics in time. One has to bear in mind that the graviton discussed in this paper is non-relativistic and massive (i.e., gapped). The closest relativistic cousin of the geometric aspects of the FQH problem is the zwei-dreibein theory of 3D massive gravity [48] (see also Ref. [49]).

In order to model the geometric quench, we utilize two recent advances in the theory of the FQH effect: the formulation of the bimetric theory [43, 50], which describes topological properties of FQH states on curved surfaces whilst incorporating the mentioned spin-2 excitation, and the generalization of the Haldane pseudopotentials [51] to systems with broken rotational invariance. Bootstrapping these methods, we derive analytical description of the real-time dynamics of FQH states following a geometric quench, and confirm it against numerical simulations for the case of Laughlin states.

Our main findings are: (i) we demonstrate that geometric quench induces the dynamics of neutral degrees of freedom in FQH states which have geometric character; (ii) in the simplest type of quenches which are driven by a mass tensor deformation in the Laughlin phase, we show that the post-quench dynamics is determined by an exponentially small fraction of excited states with quadrupolar order (i.e., spin-2) in the continuum of the spectrum, whose energy sets the oscillation frequency; (iii) we generalize the bimetric theory [43] to describe a quench, and obtain an analytical description of the dynamics following the quench [Eqs. (15) and (16)]; (iv) we show that this analytical description is in excellent agreement with exact numerical simulations of geometric quench in (ii) for finite systems at short times, and generally captures well the oscillations in the dynamics at moderate times, thus justifying the validity of bimetric theory; (v) we design more complex types of geometric quenches which excite the higher-spin excitations in the spectrum of FQH states. We note that higher-spin symmetry has attracted much interest in various areas of theoretical physics, including phase space Fermi fluid [52], collective field theory [53], generalization of gauge/gravity dualities [54], dynamics of incompressible, inviscid fluids [55, 56], large N gauge theory [57], etc. The presence of higher spin excitations in FQH states, here unambiguously identified via their distinct dynamical response, reveals a much richer structure in FQH states, including the simplest Laughlin states, and calls for an extension of their geometric description [42].

The remainder of the paper is organized as follows. In Sec. II we motivate the geometric quench and provide details of its setup. In Sec. III we introduce our method, and show that generalized pseudopotentials allow to identify states that contribute to the quench dynamics. Sec. IV contains the bulk of our numerical results for the simplest type of quench driven by changing the metric of Landau level orbitals. Analytical description of such quenches is developed in Sec. V in the framework of the bimetric theory. In Sec. VI we provide an example of a more complex type of quench which excites higher-spin modes in the spectrum, which currently lacks theoretical description. Our conclusions are presented in Sec. VII, while Appendices contain additional data and extensions of our results to more realistic (non-instantaneous) quenches and lattice models of fractional Chern insulators.

II. GEOMETRIC QUENCH OF A FRACTIONAL QUANTUM HALL STATE

The Hamiltonian describing a FQH system is given by [5]

$$H = \frac{1}{N_\Phi} \sum_{\mathbf{q}} \bar{V}_{\mathbf{q}} \bar{\rho}_{\mathbf{q}} \bar{\rho}_{-\mathbf{q}}, \tag{1}$$

where the sum runs over the 2D Brillouin zone (threaded by N_Φ flux quanta) and $\bar{\rho}_{\mathbf{q}} = \sum_{j=1}^{N} e^{i\mathbf{q}\cdot\mathbf{R}_j}$ is the density operator projected to a single Landau level (LL). The projection to a LL imposes the non-commutative geometry of the "guiding center coordinates", $\left[R_i^a, R_j^b\right] = -i\ell_B^2 \epsilon^{ab}\delta_{i,j}$, where $\ell_B = \sqrt{\hbar/eB}$ is the magnetic length [5]. This non-trivial constraint, along with the absence of kinetic energy in Eq. (1), gives rise to a wide variety of ordered phases, depending on the filling factor, $\nu = N/N_\Phi$ and the details of the (projected) interaction potential, $\bar{V}_{\mathbf{q}}$. Note that because the guiding centers do not commute, bosonic FQH states are also possible and realize a similar variety of phases [58, 59]. In this paper, we focus on the simplest Laughlin states, which occur at filling $\nu = 1/2$ for bosons and $\nu = 1/3$ for fermions.

Beside the non-commutative constraint, geometry appears in a FQH problem in three distinct guises. First,

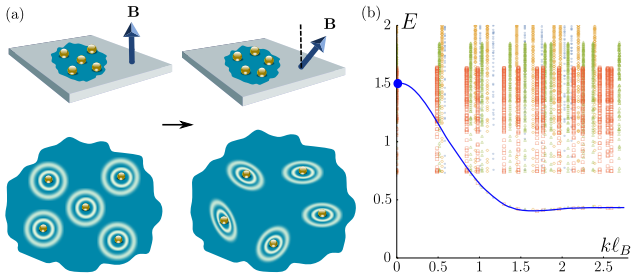

FIG. 1. (a) Geometric quench protocol: instantaneous tilt of the magnetic field induces dynamics of the intrinsic metric, which describes the shape of particle-flux composites that form a FQH state. (b) The excitation spectrum of the $\nu = 1/3$ Laughlin state, obtained by exact diagonalization of its V_1 parent Hamiltonian, in systems with $N = 7 - 10$ electrons. Blue line traces out the SMA collective mode [60], which transforms into an emergent graviton excitation in the $k \to 0$ limit (around energy $E \approx 1.5$). It will be shown in Sec. V that geometric quench induces oscillatory dynamics of the $k \to 0$ limit of the graviton mode. Note that this mode is formed by excited states in the *continuum* of the energy spectrum.

the interaction potential $\bar{V}_{\mathbf{q}} = V_{\mathbf{q}}|F_m(\mathbf{q})|^2$ is a function of two independent tensors g_m and g_i [42], where $F_m(\mathbf{q}) = \exp(-g_m^{ab} q_a q_b \ell_B^2/4)$ is the (lowest) LL form factor and $V_{\mathbf{q}}$ in general depends on $\sqrt{g_i^{ab} q_a q_b}$ (for the Coulomb interaction, $V_{\mathbf{q}} = 2\pi/\sqrt{g_i^{ab} q_a q_b}$). These two tensors are imposed by *extrinsic* experimental conditions, such as the direction of the magnetic field and properties of the underlying solid-state material. g_m has physical origin in the band mass tensor and can be conveniently parametrized by a 2×2 unimodular matrix ($\det g_m = 1$)

$$g_m = \begin{pmatrix} \cosh Q + \cos\phi \sinh Q & \sin\phi \sinh Q \\ \sin\phi \sinh Q & \cosh Q - \cos\phi \sinh Q \end{pmatrix}, \quad (2)$$

where Q and ϕ are real numbers which parametrize a stretch or rotation of the tensor. On the other hand, g_i is in general different from g_m. In the case of Coulomb interaction, g_i originates from the dielectric tensor of the material that hosts the FQH system. Note that both g_m and g_i define the shape of a circle: g_m enters the single-particle wave function thus defining the shape of LL orbitals, while g_i determines the shape of the interaction equipotentials. They hence effectively measure the distance from the "circle center", and in this sense we alternatively refer to them as extrinsic metrics [42].

Subject to these two extrinsic metrics, a FQH state develops a third, *intrinsic* geometric degree of freedom. As a many-body property of the system, this intrinsic degree of freedom defines the shape of particle-flux composite droplets in FQH ground states and can also be thought of as a metric $\hat{g}$ parametrized by the same matrix as in Eq. (2). If the extrinsic metrics are equal ($g_m = g_i$), but not necessarily isotropic ($\neq \mathbb{1}$), the intrinsic metric is equal to them ($\hat{g} = g_m = g_i$) and the physical state is isotropic in a transformed coordinate frame. More generally, when $g_m \neq g_i$, $\hat{g}$ is determined from energetic compromise between g_m and g_i, and is in general different from both of them [61, 62]. The intrinsic metric, as an emergent many-body property of the system, will be the main focus of the quench dynamics in this paper.

The dynamics of $\hat{g}$ can in principle be induced by changing the mass tensor, g_m. While this might be feasible in materials such as AlAs [63], a much more practical way is to tilt the magnetic field [Fig. 1(a)]. Semiclassically, the particles still prefer to make circular orbits around the tilted direction, but because they are confined to a narrow sample, their orbits deform into ellipses in the plane of the FQH system, hence giving rise to an effective mass anisotropy. In fact, assuming parabolic confining potential in the perpendicular direction, tilt can be exactly represented as a 2×2 anisotropic mass tensor [61, 64, 65]. Hence, to an excellent approximation we can model the effect of a tilt by an anisotropic mass tensor like in Eq. (2) [64].

Our quench protocol can now be defined as follows: (i) prepare a Laughlin state $|\psi_0\rangle$ as the ground state of H with mass tensor g_m; (ii) instantaneously change $g_m \to g'_m$; (iii) evolve in time assuming the system is closed, i.e., $|\psi(t)\rangle = \exp(-iH't)|\psi_0\rangle$, and measure the intrinsic metric as a function of time, $\hat{g}(t)$. This protocol is the minimal theoretical model for an experiment where the magnetic field is suddenly tilted. At considerable computational expense, the model can be made more realistic by directly including parallel field (instead of approximating it by mass anisotropy), relaxing the assumption of a closed system, etc. In later sections of the paper, we will consider some generalizations of the protocol where the quench cannot be described in terms of 2×2 metric (Sec. VI) or when it is not applied instantaneously (Appendix C).

The intuition behind geometric quench is the following. In a purely perpendicular field, a FQH state is a low-entangled state of composite objects – particles surrounded by correlation holes of certain size. For example, in the $\nu = 1/3$ Laughlin state we can view them as electrons in an area corresponding to three magnetic flux quanta [Fig. 1(a)]. These objects have a finite area (fixed by the electron density and total flux through the system), but their shape can vary and is determined by the intrinsic metric $\hat{g}$ of the FQH state [66], or equivalently by two real parameters, Q and ϕ, as in Eq. (2). For a weak quench that keeps the system within the Laughlin phase, these droplets are expected to fluctuate and our goal is to determine the equations of motion for Q and ϕ. This is, however, a highly non-trivial problem because the representation of a state in Fig. 1(a) is merely a cartoon (e.g., the operators projected onto the droplets do not commute with one another).

As emphasized earlier, the key to understanding dynamics are the excited eigenstates in the spectrum of H'. Such a spectrum for the Laughlin $\nu = 1/3$ state, obtained by diagonalization of its parent Hamiltonian – the V_1 Haldane pseudopotential [67]– is shown in Fig. 1(b). The low-energy spectrum is dominated by a collective mode

known as the Girvin-MacDonald-Platzman (GMP) mode or "magnetoroton" [60, 68]. This mode is accurately described by the single-mode approximation (SMA), and intuitively represents a density modulation on top of the ground state given by $\bar{\rho}_{\mathbf{k}}|\psi_0\rangle$. Such SMA trial wavefunctions were shown to give excellent description of the actual collective excitation for momenta smaller than the magnetoroton minimum [69], both for the exact Laughlin state and the Coulomb ground state. Generalizations of the SMA, based on Jack polynomials, have been shown to be microscopically accurate at *all* values of momenta accessible in finite systems [70].

Since the SMA dominates the low-energy physics of a FQH state, it could be expected that it also plays a crucial role in the quench dynamics. However, this becomes less clear if one notices that our quench protocol preserves the translation symmetry of the initial state, hence all dynamics takes place in $\mathbf{k} = 0$ sector of the Hilbert space that contains the uniform Laughlin state. The $k \to 0$ limit of the SMA mode, i.e., the spin-2 graviton [70], lies inside the 2 quasiparticle-2 quasihole continuum of states [Fig. 1(b)], hence it is far from obvious that quench dynamics can be modelled by this single degree of freedom (although in some cases the $k \to 0$ limit of the SMA mode mode appears to be below the continuum of the energy spectrum [71]). In the following Section, we present results of exact numerical simulations of the quench dynamics in finite-size systems. These results will show that the simplest type of geometric quench described by Eq. (2) indeed gives rise to coherent oscillations of the geometric spin-2 degree of freedom for the Laughlin state. We note, however, that more general types of quenches are also possible, which cannot be mapped to a simple modification of the mass tensor. These quenches, which will be considered in Sec. VI, excite the tower of higher spin modes in the spectrum of a FQH state, giving rise to non-trivial dynamics which is not captured by the simple graviton oscillation.

III. METHOD

We model the quench by performing numerically exact time evolution with the Hamiltonian in Eq. (1) defined for N particles and N_Φ flux quanta on a square torus [Fig. 2(a)]. Magnetic translation symmetry [72] is used to reduce the complexity of the calculation and to classify the many-body eigenstates. We focus on the Laughlin states of bosons and fermions, corresponding to filling factors $\nu = 1/2$ and $\nu = 1/3$, respectively.

We consider two types of interaction potentials. In the first case, we assume model (short-range) interaction for which the Laughlin state is the unique (and the densest) zero-energy state [73]. This interaction is a simple contact repulsion for bosons, $V_{\mathbf{q}} = 1$, and for fermions it is $V_{\mathbf{q}} = L_1(g_m^{ab} q_a q_b)$, where L_1 is the first Laguerre polynomial. As customary in the literature [42], in the model interaction we have assumed that the interaction metric

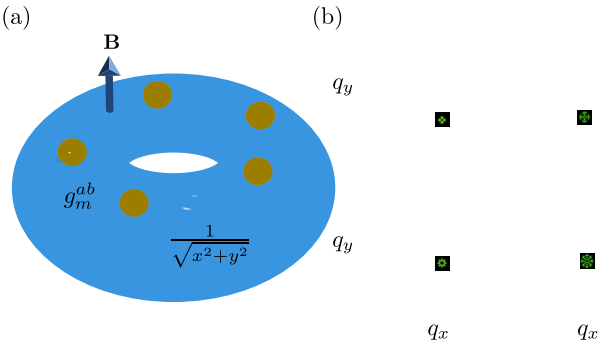

FIG. 2. (a) A FQH system on the surface of a torus threaded by perpendicular magnetic field. The mass tensor g_m determines the metric of the Landau level orbitals and is used to drive a quench, while the Coulomb potential is assumed to be isotropic. (b) Contours in momentum space of the leading order anisotropic pseudopotentials for bosons [51] with quadrupolar ($V_{0,2}$, $V_{2,2}$) and octupolar ($V_{0,4}$, $V_{2,4}$) structure.

g_i coincides with the Landau orbit metric g_m. In the second case, we consider Coulomb interaction, for which g_i is kept isotropic, i.e., $V_{\mathbf{q}} = 2\pi/\sqrt{q_x^2 + q_y^2}$, but the mass tensor g_m is allowed to be non-isotropic.

For both types of interaction, the quench is implemented by switching g_m to g'_m at time $t = 0$, where both g_m and g'_m, for simplicity, are taken to be diagonal, like in Eq. (11) below. For small system sizes, the subsequent time evolution is performed by obtaining all energy eigenvalues ϵ_n and corresponding eigenvectors $|n\rangle$ of the quench Hamiltonian H', and then evaluating $|\psi(t)\rangle = \sum_n \exp(-i\epsilon_n t)\langle n|\psi_0\rangle|n\rangle$. By restricting the sum to a subset of eigenstates, one can conveniently project the dynamics onto a desired energy shell. At larger system sizes, we use time-dependent Lanczos methods to iteratively compute $|\psi(t)\rangle$.

We use the same parametrization for the intrinsic metric $\hat{g}$ as in Eq. (2). Due to its invariance under $Q \to -Q$ and $\phi \to \phi + \pi$, we focus on $Q \geq 0$. For a given state $|\psi(t)\rangle$, $\hat{g}$ is determined by brute force search over a large set of (precomputed) trial states $|\psi_{\text{trial}}\rangle$, i.e., model Laughlin states parametrized by $Q \in [0, Q_{\max}]$ and $\phi \in [-\pi, \pi]$, such that the overlap $|\langle\psi_{\text{trial}}|\psi(t)\rangle|$ is maximized. For weak quenches, we found it sufficient to restrict to $Q_{\max} = 1$ and $\phi \in [-\pi/2, \pi/2]$. The confidence in the result is quantified by the maximum overlap achieved: if this overlap is not close to 1 (like in the case of strong quench), none of the trial states appropriately describes the system and the intrinsic metric should be determined via some other means, for example via minimization of the total energy or momentum polarization [74].

Finally, in order to identify states corresponding to the spin-n excitation, we use the recently developed formalism of anisotropic pseudopotentials [51]. In Ref. [51] it was shown that any two-particle interaction, including cases where metrics g_m and g_i are different, can be

expanded into an orthonormal basis of generalized pseudopotentials. These operators maintain translation invariance, but break rotation symmetry to a discrete subgroup. Up to normalization prefactors, the generalized pseudopotentials are given by [51]

$$V_{m,n}\left(g_p; q_x, q_y\right) = L_m^n\left(g_p^{ab} q_a q_b\right) \mathbf{q}^n + \text{c.c}, \tag{3}$$

where m, n are even integers (for bosons). When $n = 0$, these reduce to the usual (isotropic) Haldane pseudopotentials [73]. $V_{m,n}$ explicitly depends on the metric g_p through the argument of the Laguerre polynomial, as well as the vector $\mathbf{q}$. For simplicity, we fix $g_p = \mathbb{1}$ and $\mathbf{q} = \frac{1}{\sqrt{2}}(q_x + iq_y)$ in our numerics.

Contours of leading-order $V_{m,n}$ for bosons are depicted in Fig. 2(b). In particular, we can observe that the dominant pseudopotential $V_{0,2}$ has a clear quadrupolar structure in momentum space, indicating that $\hat{V}_{0,2}$ carries angular momentum $L_z = 2$. Based on this, we use $\hat{V}_{0,n}$ as a spectroscopic probe to identify many-body eigenstates which are part of the effective spin-n excitation. To that end, we introduce the following "spectral function":

$$I_{m,n}(\omega) = \sum_j \delta(\omega - \epsilon_j)|\langle j|\hat{V}_{m,n}|0\rangle|^2, \tag{4}$$

where ϵ_j and $|j\rangle$ are the eigen-energy and eigenstate of Eq. (1). This is a generalization of the spectral function that describes an acoustic wave absorption experiment [75]. The peaks of $I_{m,n}$ can be used to obtain the frequencies of different spin modes in the quench dynamics. In the following Section, we investigate in detail $I_{0,2}$ and show that it indeed yields the frequency of the graviton mode.

IV. RESULTS

Here we present our numerical results for weak quenches, where the mass tensor is instantaneously changed from $g_m = \text{diag}(e^{A_0}, e^{-A_0})$ to $g'_m = \text{diag}(e^{A_1}, e^{-A_1})$ with A_0 and A_1 close to 0. By "weak" quench we mean that the system remains in the Laughlin phase. Note that this does not imply that we restrict to an infinitesimal variation of the parameters in the Hamiltonian. Indeed, the parameters of our quenched Hamiltonian differ by a finite amount from the original Hamiltonian, which allows the dynamics to explore a finite density of excitations.

In the following, we focus on the dynamics of $\hat{g}$ for $\nu = 1/2$ bosons in detail, while similar results for $\nu = 1/3$ fermions are given in Appendix D. In all numerical data below, time is given in units of inverse energy [$e^2/(\epsilon \ell_B)$ in the case of Coulomb interaction], with $\hbar = 1$.

A. Isotropic-to-anisotropic quench

We start with the simple case of $A_0 = 0, A_1 > 0$, where the initial state is the isotropic Laughlin state.

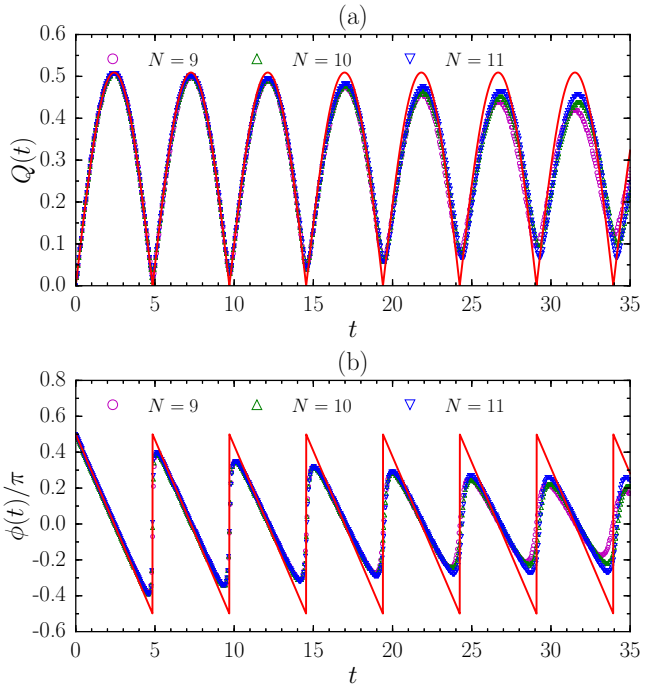

FIG. 3. Exact dynamics of (a) Q and (b) ϕ for $N = 9 - 11$ bosons at $\nu = 1/2$ with the contact interaction. The quench is driven by choosing $A_0 = 0$ and $A_1 = \ln 1.3$. The red curves are fits to Eqs. (5) and (6), which coincide with the predictions of the bimetric theory, discussed in Sec. V.

As representative examples, we choose $A_1 = \ln 1.3$ and $A_1 = \ln 2.0$ for quenches driven by contact and Coulomb interactions, respectively. The intrinsic metric $\hat{g}$ of the post-quench state is determined by the maximum of the overlap between the post-quench state and a trial set of anisotropic Laughlin states. The regime of weak quench corresponds to the maximum of this overlap being close to unity. Exact dynamics of $\hat{g}$ up to moderate times is shown in Figs. 3 and 4 for the two types of interactions. We observe that both Q and ϕ oscillate with a well-defined frequency (and in particular, ϕ appears to be a *linear* function of time). This is rather surprising because the induced change in the microscopic structure of the FQH state is by no means small: for the above choices of A_1 in Figs. 3 and 4, we find the maximum anisotropy e^Q of the post-quench state to be larger than the initial (isotropic) state by a factor $1.5 - 2.5$.

Assuming a single harmonic, we might guess that the oscillations in Figs. 3 and 4 are well described by

$$Q(t) = 2A \sin\left(\frac{E_\gamma t}{2}\right), \quad \phi(t) = \frac{\pi}{2} - \frac{E_\gamma t}{2}, \tag{5}$$

$$Q(t) = -2A \sin\left(\frac{E_\gamma t}{2}\right), \quad \phi(t) = \frac{3\pi}{2} - \frac{E_\gamma t}{2}, \tag{6}$$

where Q obeys harmonic motion and ϕ has a simple linear dependence on time. Note that only one of these two solutions is independent because the system is invariant

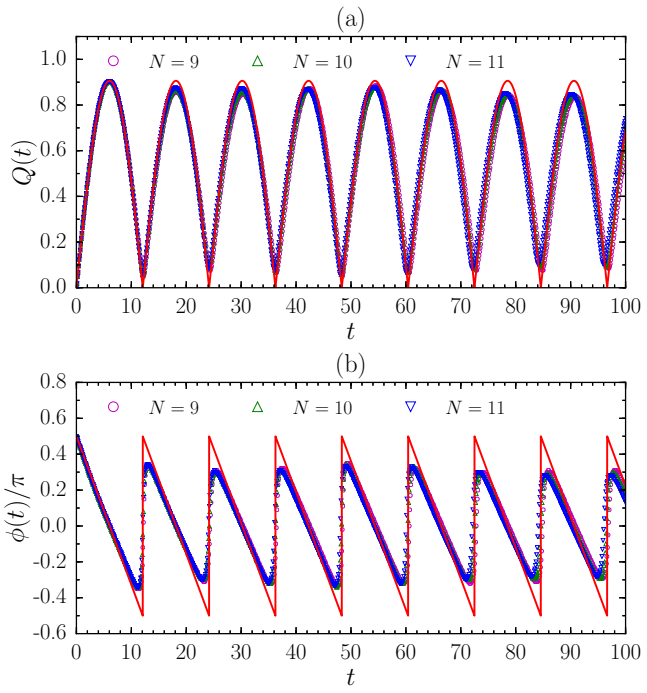

FIG. 4. Exact dynamics of (a) Q and (b) ϕ for $N = 9 - 11$ bosons at $\nu = 1/2$ with the Coulomb interaction. The quench is driven by choosing $A_0 = 0$ and $A_1 = \ln 2.0$. The red curves are fits to Eqs. (5) and (6), which coincide with the predictions of the bimetric theory, discussed in Sec. V.

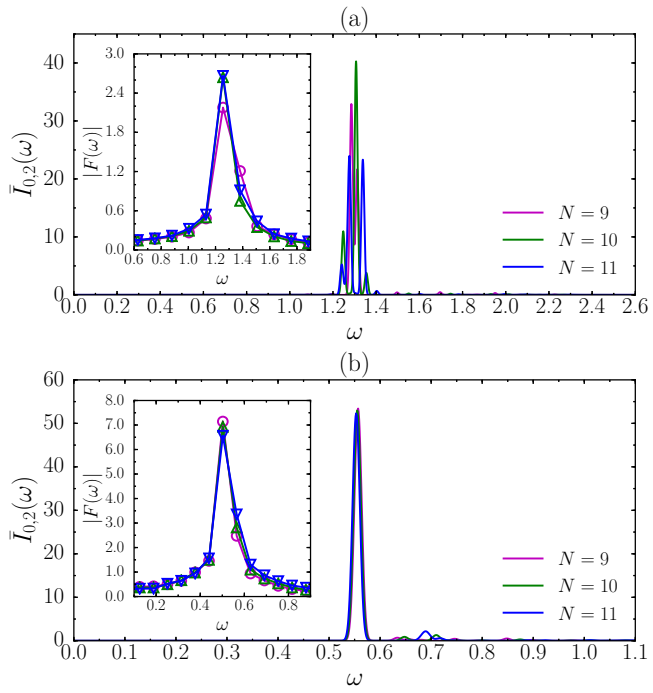

FIG. 5. Normalized spectral function $\bar{I}_{0,2}(\omega) = I_{0,2}(\omega)/\int I_{0,2}(\omega)d\omega$ for isotropic systems of $N = 9-11$ bosons at $\nu = 1/2$ with (a) contact and (b) Coulomb interactions. The insets show the discrete Fourier transform $|F(\omega)|$ of Q in Figs. 3 and 4. Markers in insets and curves in main figures with the same color refer to the same system size.

under $Q \to -Q$ and $\phi \to \phi + \pi$. Thus, we can focus on the $Q \geq 0$ part and consider ϕ mod 2π. By inspection of $Q(t)$, we see the solution will alternate between the two branches, which doubles the frequency from $E_\gamma/2$ to E_γ. The overall prefactor (written as $2A$) is expected to be proportional to the intrinsic anisotropy of the state.

Fitting the first one or two oscillations in Figs. 3 and 4 against Eq. (5) yields remarkably accurate agreement with full dynamics across the entire time interval. What sets the frequency, E_γ, of the oscillations? From the fits, we obtain $E_\gamma \approx 1.296$ and 0.520 for the cases of contact and Coulomb interactions, respectively. These values do not match the spectral gap in the $\mathbf{k} = 0$ momentum sector, which can be much smaller (see Fig. 1). Instead, as shown below, they agree with the *graviton* gap very well, which we *independently* estimate to be ≈ 1.3 for the contact interaction and 0.52 for the Coulomb interaction.

In order to justify the identification of E_γ with the graviton gap, we use $I_{0,2}(\omega)$ spectral function defined in Eq. (4) to detect the states that carry spin-2. We expect peaks of $I_{0,2}(\omega)$ at energies corresponding to the spin-2 excitations that comprise the graviton mode. In Fig. 5, we show $I_{0,2}(\omega)$ (normalized by $\int I_{0,2}(\omega)d\omega$) for contact and Coulomb interactions in isotropic systems (similar data are obtained for weakly anisotropic systems). In the case of contact interaction, we observe sharply pronounced peaks of $I_{0,2}(\omega)$ around $\omega = 1.3$ for various system sizes [Fig. 5(a)], which means that spin-2 eigenstates concentrate in this narrow energy window, corresponding to the graviton gap $E_\gamma \approx 1.3$. For Coulomb interacting systems, a pronounced peak in $I_{0,2}(\omega)$ also exists, but at a lower energy $\omega = 0.55$ [Fig. 5(b)]. As an independent estimate of the graviton gap, we use the discrete Fourier transform of Q (see insets of Fig. 5). This Fourier transform also shows a sharp peak around the same energy as that in $I_{0,2}(\omega)$, which further confirms that the dynamics of the intrinsic metric is indeed caused by the graviton oscillation.

B. States contributing to dynamics

The agreement between the oscillation frequency in the exact dynamics of $\hat{g}$ and the graviton gap strongly implies that the dynamics is dominated by spin-2 eigenstates of H'. We now scrutinize this conjecture by quantifying how well the full dynamics can be reproduced by an explicit projection to the subset of eigenstates centered around the the energy of the spin-2 mode.

The projected subspace is defined by the eigenstates $|n\rangle$ of H' with dominant matrix elements $|\langle n|\hat{V}_{0,2}|0\rangle|^2$. The weight of this projection is measured by

$$f = \left(\sum_{n=0}^{M-1} |\langle n|\hat{V}_{0,2}|0\rangle|^2\right) / \left(\sum_{n=0}^{D-1} |\langle n|\hat{V}_{0,2}|0\rangle|^2\right), \quad (7)$$

where $|n\rangle$ have been sorted in descending order according to $|\langle n|\hat{V}_{0,2}|0\rangle|^2$. Here M is the number of kept states and D is the total number of eigenstates that we can obtain from exact diagonalization of H', i.e., D is equal to the Hilbert space dimension in the $\mathbf{k}=0$ sector for $N \leq 9$, while for practical reasons we kept $D = 200$ for larger systems ($N = 10-12$). Remarkably, the number of states we need to saturate the total weight f is significantly smaller than the Hilbert space dimension. Fixing $f = 99\%$, the finite-size scaling of the required M clearly indicates that only an exponentially small fraction of the whole Hilbert space carries spin-2, as seen in Fig. 6.

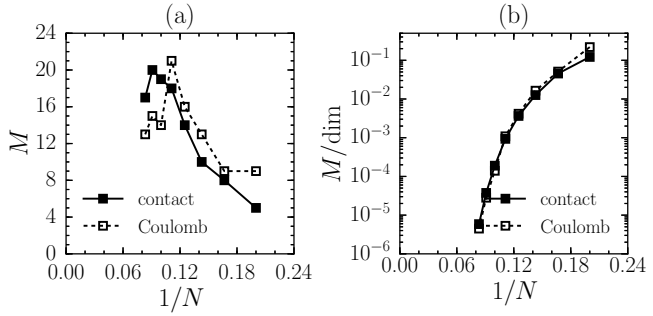

FIG. 6. Finite-size scaling of the number of spin-2 states in the $\mathbf{k}=0$ Hilbert space for $N = 5-12$ bosons at $\nu = 1/2$. M represents the number of states which contain $f = 99\%$ of the total $|\langle n|\hat{V}_{0,2}|0\rangle|^2$. We consider both contact and Coulomb quench Hamiltonians, with $A_1 = \ln 1.3$ and $A_1 = \ln 2.0$, respectively. The plots show (a) M and (b) M/dim, where dim is the $\mathbf{k}=0$ Hilbert space dimension.

While the exponentially decaying ratio of M to the Hilbert space dimension might not be entirely surprising (since it still does not preclude M being exponentially large in the system size), it can also be shown that, in absolute terms, only a very small number of states M yields a very accurate approximation to the exact dynamics. In Appendix B, we perform the above projection, based on the $|\langle n|\hat{V}_{0,2}|0\rangle|^2$ matrix elements, for the dynamics of $N = 11$ bosons driven by the isotropic-to-anisotropic quench (Fig. 10). Remarkably, the main features of the exact dynamics are already accurately reproduced for M less than 10, even if there are as many as 533160 eigenstates in the entire $\mathbf{k}=0$ Hilbert space. Such an excellent approximation of the exact dynamics by an exponentially small fraction of states in the Hilbert space is further evidence for the picture of graviton oscillation.

V. WEAK GEOMETRIC QUENCH IN BIMETRIC THEORY

In the previous Section, we have established that quenching the mass tensor, Eq. (2), in the Laughlin phase gives rise to dynamics which is supported over a vanishingly small fraction of states that carry spin-2. Thus, we expect that our results in Sec. IV can be used to test the validity of the bimetric theory [43]. Here we generalize the bimetric theory to anisotropic quantum Hall states, and derive an analytical description of the dynamics of the intrinsic metric $\hat{g}$ after a quench exciting spin-2 states. We find that this analytical prediction agrees remarkably well with the exact numerics of geometric quench in Sec. IV, which strongly supports the validity of the bimetric theory. Despite of its agreement with the bimetric theory in special quenches exciting spin-2 states, we should emphasize that geometric quench is a logically independent method and contains much new physics beyond the bimetric theory (see Sec. VI).

A. Lagrangian for the isotropic case

Bimetric theory describes gapped dynamics of a single spin-2 degree of freedom in a FQH system, interacting with an external electro-magnetic field and ambient geometry. The dynamical degree of freedom is the vielbein $\hat{e}_i^\alpha$ [76] that "squares" to the dynamic, unimodular metric $\hat{g}_{ij} = \hat{e}_i^\alpha \hat{e}_j^\beta \delta_{\alpha\beta}$, or simply $\hat{g} = \hat{e}\cdot\hat{e}^T$. Here $\hat{g}$ corresponds to the intrinsic metric of the FQH state mentioned in Sec. II. The inverse metric is given by $\hat{G}^{ij} = \hat{E}_\alpha^i \hat{E}_\beta^j \delta^{\alpha\beta}$, where $\hat{E}_\alpha^i$ is the inverse vielbein [76], satisfying $\hat{E}_\alpha^i \hat{e}_j^\alpha = \delta_j^i$. The unimodular condition on $\hat{g}_{ij}$ takes form $\sqrt{g} = \sqrt{\hat{g}}$, where $\sqrt{g}$ is the determinant of the *ambient* metric $g_{ij} = \delta_{AB} e_i^A e_j^B$ and e_i^A is the ambient vielbein. Thus, in flat ambient space (that is, when $g_{ij} = \delta_{ij}$), $\sqrt{\hat{g}} = 1$.

In the absence of an external electric field, and when the magnetic field is homogeneous, the Lagrangian takes form [43]

$$\mathcal{L} = \frac{\nu\varsigma}{2\pi\ell_B^2}\hat{\omega}_0 - \frac{m}{2}\left[\frac{1}{2}\hat{g}_{ij}g^{ij} - \gamma\right]^2 = \mathcal{L}_{\mathrm{top}} + \mathcal{L}_{\mathrm{pot}}\,, \quad (8)$$

where $\hat{\omega}_0$ is the temporal component of the (dynamic) Levi-Civita spin connection, given by

$$\hat{\omega}_0 = \frac{1}{2}\epsilon_\alpha{}^\beta \hat{E}_\beta^i \partial_0 \hat{e}_i^\alpha\,. \quad (9)$$

The phenomenological coefficient m sets the energy scale which determines the gap of the spin-2 mode. Quantized coefficient ς is determined by the "shift" $\mathcal{S}$ [43] and takes the value $|\varsigma| = \frac{|\mathcal{S}-1|}{2}$. The phenomenological parameter γ is used to tune the theory close to the nematic phase transition, where the SMA is exact, in the gapped phase $\gamma < 1$. Futher details on the bimetric Rieman-Cartan geometry can be found in Refs. [43, 74]. We will utilize it to introduce anisotropy into the problem.

B. Anisotropy in bimetric theory

To introduce the quadrupolar anisotropy from a nontrivial mass tensor or other sources, we take the inspiration from Ref. [74], where quadrupolar anisotropy was

described in geometric terms. More concretely, we introduce a unimodular matrix m_{AB}, and construct a rank-2 tensor from it according to

$$g_{ij}^{(\mathrm{m})} = \mathrm{m}_{AB} e_i^A e_j^B \,, \tag{10}$$

where e_i^A are the vielbeins that describe the ambient geometry. We now generalize Eq. (8) to the anisotropic case. To do so we simply replace g_{ij} by $g_{ij}^{(\mathrm{m})}$ in Eq. (8).

To analyze the theory further we make the following simplifying assumptions: (i) the ambient space is assumed to be flat, $e_i^A = \delta_i^A$, and (ii) we assume a particular parametrization of $g_{ij}^{(\mathrm{m})}$, given by

$$g_{ij}^{(\mathrm{m})} = \begin{pmatrix} e^A & 0 \\ 0 & e^{-A} \end{pmatrix} , \tag{11}$$

where A is a real parameter that defines the effective anisotropy in the FQH system, which is a compromise between two extrinsic metrics g_m and g_i as discussed in Sec. II. The abrupt change of the mass tensor g_m in our quench protocol will lead to the change of A in Eq. (11).

In order to compute the dynamics of $\hat{g}_{ij}$, we parametrize it in terms of Q and ϕ as in Eq. (2). Both Q and ϕ are functions of time, but not space, since the problem we will consider is homogeneous (i.e., the quench is global). The two terms in the Lagrangian take the form

$$\mathcal{L}_{\mathrm{top}} = \frac{\varsigma\bar{\rho}}{2} (1 - \cosh Q)\, \dot{\phi} \,, \tag{12}$$

$$\mathcal{L}_{\mathrm{pot}} = -\frac{m}{2} (\gamma + \sinh A \sinh Q \cos\phi - \cosh A \cosh Q)^2 \,. \tag{13}$$

The equations of motion are found from

$$\frac{\delta S}{\delta \phi} = 0 \,, \qquad \frac{\delta S}{\delta Q} = 0 \,, \tag{14}$$

where $S = \int d^3x\, \mathcal{L}$ is the action. The equation for $\phi(t)$ takes the form

$$\dot{\phi} \sinh Q = -2\Omega \left(\sinh A \cosh Q \cos\phi - \cosh A \sinh Q\right) \left(\gamma + \sinh A \sinh Q \cos\phi - \cosh A \cosh Q\right) \,, \tag{15}$$

and for $Q(t)$ we find

$$\dot{Q} \sinh Q = -2\Omega \sin\phi \sinh Q \sinh A \left(\gamma + \sinh A \sinh Q \cos\phi - \cosh A \cosh Q\right) \,, \tag{16}$$

where we have introduced the energy scale $\Omega = \frac{m}{\bar{\rho}\varsigma}$. Eqs. (15) and (16) are the central result of this Section.

C. Isotropic limit

In the isotropic case we must take $A \to 0$. We find

$$\dot{Q} = 0 \,, \qquad \dot{\phi} = 2\Omega \left(\gamma - \cosh Q\right) \,. \tag{17}$$

Choosing the solution $Q = 0$ of the first equation, the second equation reads

$$\dot{\phi} = -2\Omega(1-\gamma) \equiv -E_\gamma \quad \Rightarrow \quad \phi(t) = \phi(0) - E_\gamma t \,, \tag{18}$$

from where we interpret $E_\gamma = 2\Omega(1-\gamma) = \frac{2m(1-\gamma)}{\bar{\rho}\varsigma}$ as the gap of the spin-2 part of the GMP mode at $\mathbf{k} = 0$ [43]. When $\gamma \to 1$, the gap closes and the FQH state undergoes a nematic phase transition [43]. The dynamical metric evaluated on this solution takes the form

$$\hat{g}_{ij} = \begin{pmatrix} 1 & 0 \\ 0 & 1 \end{pmatrix} , \tag{19}$$

consequently the dynamics of $\phi(t)$ is not visible in the fluctuations of the dynamical metric. Formally speaking, this happens because $Q = 0$. When Q is different from 0 the metric will be sensitive to the dynamics of ϕ. This is what happens in the case of weak anisotropy discussed next.

D. Weak geometric quench in bimetric theory

In order to perform the quench, we have to phrase it in terms of Eqs. (15) and (16). Taking inspiration from Ref. [77], we perform the quench in two steps. First, we need to fix the initial condition $Q(0), \phi(0)$ for Eqs. (15) and (16), which should be determined by the intrinsic metric of the initial Laughlin state $|\psi_0\rangle$. Second, to obtain the quench dynamics, we solve Eqs. (15) and (16) under such initial condition, with the value of A determined by the effective anisotropy of H' (or equivalently, by the intrinsic metric of the ground state of H').

When anisotropy is weak, we can assume both A and Q are close to 0. Taylor expansion of Eqs. (15) and (16) in A and Q leads to the following system of linear equations

$$\dot{\phi} Q = E_\gamma \left(A \cos\phi - Q\right) \,, \tag{20}$$

$$\dot{Q} = E_\gamma A \sin\phi \,, \tag{21}$$

for which analytical solutions exist under suitable initial conditions. In particular, for $Q(0) = 0$, it can be verified by direct substitution that our earlier Eqs. (5)-(6), which were used to fit the numerical data in Sec. IV, are exact solutions.

As long as the quench is weak, the linearized Eqs. (20) and (21) provide a very accurate approximation to the full non-linear dynamics. Fig. 7 shows the comparison of

the numerical solutions of non-linear Eqs. (15) and (16) satisfying $Q(0) = 0$ against their linearized counterparts, Eqs. (5) and (6), where we focus on the $Q \geq 0$ part and consider ϕ mod 2π. Red solid lines in Fig. 7 result from a combination of Eqs. (5) and (6), which gives us Q and ϕ as periodic functions with frequency E_γ. Mathematically, it is rather surprising that Eqs. (5)-(6) display such close agreement with the solutions of Eqs. (15) and (16), since the latter appear to be strongly non-linear.

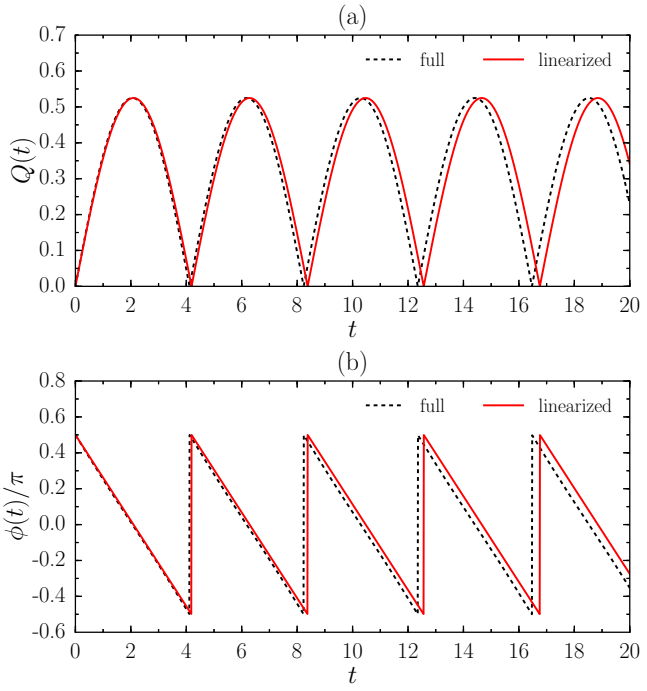

FIG. 7. Predictions of the bimetric theory for (a) Q and (b) ϕ under the initial condition $Q(0) = 0$. Black dashed lines indicate the numerical solution of the full equations, Eqs. (15) and (16). Red solid lines indicate the analytical solution Eqs. (5) and (6) of the linearized system, Eqs. (20) and (21). Here we focus on the $Q \geq 0$ solution. The parameters are fixed at $\Omega = 1.5/4$, $\gamma = -1$, $A = \ln 1.3$.

E. Agreement between bimetric theory and exact dynamics

Since Eqs. (20)-(21) are an accurate approximation of Eqs. (15)-(16) in the weak quench regime, we were justified in fitting our exact results in Sec. IV against simple harmonic oscillation in Eqs. (5)-(6). The fits allow us to extract the values of A and E_γ, which we can now interpret as the intrinsic anisotropy and graviton gap in the bimetric theory.

By extracting E_γ from the fitting of quench data for various initial parameters, we indeed find that the obtained E_γ is insensitive to the precise values of A_0 and A_1, as long as we are in the weak quench regime. On the other hand, A quantifies the intrinsic anisotropy in the ground state of H', which is a compromise between g'_m and g'_i. Since we do the same modification for g_m and g_i in the quench driven by the contact interaction, we expect $A = A_1$ in this case. Indeed, we get $A \approx 0.255$ from the fit in Fig. 3, which is very close to $A_1 = \ln 1.3 \approx 0.262$. However, in the quench driven by the Coulomb interaction, we keep isotropic g_i and only change g_m, so the intrinsic anisotropy in the ground state of H' is expected to be weaker than g'_m. The fit in Fig. 4 gives $A \approx 0.454$, which is indeed between 0 and $A_1 = \ln 2.0 \approx 0.693$.

In summary, we find that weak isotropic-anisotropic mass anisotropy quenches in the Laughlin phase can be described as harmonic motion of a single spin-2 degree of freedom, in agreement with the bimetric theory. Minor deviations from harmonic motion can be observed in Figs. 3 and 4 at longer times. These deviations generally have two manifestations: as a decay in amplitude while maintaining the overall oscillation structure, or as a total departure from the oscillation. The former is mainly the case for isotropic-to-anisotropic quenches considered in Figs. 3 and 4, while the latter can be observed in a more general case of anisotropic-to-anisotropic quench considered in Appendix A as well as in some fermionic data in Appendix D.

There are several possible explanations for the discrepancy with the bimetric theory. First, in finite systems a "fragmentation" of the spin-2 graviton mode into several states with large matrix element $|\langle n|\hat{V}_{0,2}|0\rangle|^2$ (as seen in Fig. 5) induces several close frequencies in the dynamics. With the available data for system sizes up $N = 12$, there is no clear indication that this fragmentation disappears in the thermodynamic limit, even though a "sharp" spin-2 mode is theoretically anticipated in large systems. This suggests that finite size effects, to the zeroth order, do not seem to be the explanation for the fragmentation. Note that the fragmentation for the Coulomb interaction is much weaker than that for the contact interaction (Fig. 5), reflecting a more isolated graviton mode in the Coulomb case. A more likely source of "finite-time" errors in the dynamics could be due to an effective Lieb-Robinson [78] "light cone" exceeding the finite size of the system. Finally, the discrepancy could arise due to the contribution of higher-spin modes to the dynamics. In the following Section, we design more complex type of quenches to probe such modes. These quenches lead to non-trivial dynamics which is not accounted for in the bimetric theory or its direct extensions in Eqs. (5)-(6).

VI. HIGHER-SPIN MODES

A. W_∞ algebra in the lowest Landau level

It has been realized a long time ago that the lowest Landau level admits an action of the (infinite-dimentional) algebra of area-preserving diffeomorphisms (APD), W_∞ [68, 79]. The action of this algebra can be interpreted as area-preserving distortions of FQH droplets

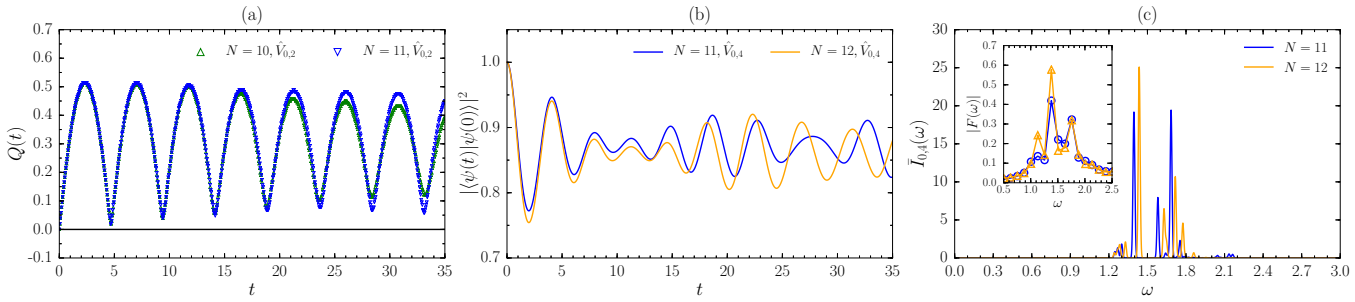

FIG. 8. (a) Exact dynamics of Q for the quench with $\hat{V}_0 \to \hat{V}_0 + 0.1\hat{V}_{0,2}$ (color symbol) and $\hat{V}_0 \to \hat{V}_0 + 0.1\hat{V}_{0,4}$ (black solid line). A complete absence of dynamics of $\hat{g}$ can be noticed in the case of the pertubation by $\hat{V}_{0,4}$. (b) Dynamics of quantum fidelity, $|\langle\psi(t)|\psi(0)\rangle|^2$, for the quench with $\hat{V}_0 \to \hat{V}_0 + 0.1\hat{V}_{0,4}$. (c) Normalized spectral function $\bar{I}_{0,4}(\omega) = I_{0,4}(\omega)/\int I_{0,4}(\omega)d\omega$ for isotropic systems of $N = 11$ and 12 bosons at $\nu = 1/2$ with contact interaction. The inset shows the discrete Fourier transform $|F(\omega)|$ of $|\langle\psi(t)|\psi(0)\rangle|^2$. Markers in insets and curves in main figures with the same color refer to the same system size.

illustrated in Fig. 1. These distortions, however, cost finite energy since the interaction potential, Eq. (1), is not invariant under these transformations [42, 68]. Consequently, the gapped spin-2 mode discussed in the previous section can be viewed as a particular, quadrupolar, APD of the droplet. This fact is reflected in the bimetric theory, in the form of hidden $sl(2,\mathbb{R})$ (which is the largest finite-dimensional subalgebra of W_∞) symmetry [43]. Topological part of the action in Eq. (8) is invariant under the action of $sl(2,\mathbb{R})$, while the Hamiltonian explicitly breaks it down to $so(2) \subset sl(2,\mathbb{R})$. Thus, the application of the (broken) shear generators of $sl(2,\mathbb{R})$, represented by the off-diagonal components of the emergent metric $\hat{g}_{ij}$, leads to the creation of an excited spin-2 state.

Naturally, one may expect that higher angular momentum distortion of the fluid will correspond to independent collective modes, at least at long wavelengths [80, 81]. Construction of an effective theory describing the infinite number of interacting higher spin-fields is not an easy task, and has been an outstanding problem for a long time. A significant advance in solving this problem in $(2+1)D$ was made in [82, 83], where Chern-Simons-type action for higher spin gravity was constructed. Presently, it is not understood how these ideas can be applied to the FQH problem.

The algebra of APDs made multiple appearances in the FQH problem: non-commutative Chern-Simons theory [84], matrix models [85, 86], bosonization of the LLL problem [87], manifestly LLL-projected description of the CFL-type state of bosons at $\nu = 1$ [88]. Higher-spin degrees of freedom naturally appear in the composite fermion approach to the Jain series at filling $\nu = \frac{n}{2n+1}$, at large values of n (i.e., close to half-filling) [50, 81]. Those theories describe free massive higher spin fields with a quadratic action. Consequently, the (inherently non-linear) W_∞ structure is invisible. In what follows we provide evidence, obtained directly from the microscopic quench dynamics, that at long distances the electrons forming a FQH fluid support collective modes of higher spin. The evidence is obtained by designing a quench protocol that selectively excites the higher-spin collective modes.

B. Higher-spin quench

Tuning the anisotropy of the mass tensor is an experimentally relevant mechanism for changing the metric in the interaction. However, this also leads to the modification of the entire set of coefficients $c_{m,n}$ of the generalized Haldane pseudopotentials $\hat{V}_{m,n}$ [Eq. (3)], which uniquely characterize the interaction:

$$\bar{V}_{\mathbf{q}} = \sum_{m,n} c_{m,n} V_{m,n}(\mathbf{q}). \tag{22}$$

Modifying individual coefficients $c_{m,n}$, one at a time, is a much more controlled way to drive a quench. While this may not be easily achievable in experiment, this new quench protocol allows for more control in probing different types of dynamics. As we show below, reformulating the quench protocol in this way not only includes the former scenario of changing the mass tensor, but also reveals new types of dynamics, which lie beyond the single mode approximation and the bimetric theory.

To perform the quench we prepare a state annihilated by the Hamiltonian with $c_{m,n} = \delta_{n,0}\delta_{m,0}$. Then, a nonzero $c_{0,2} = 0.1$ is introduced at $t = 0^+$. This corresponds to the modification of the interaction $\hat{V}_0 \to \hat{V}_0 + 0.1\hat{V}_{0,2}$. Since $\hat{V}_{0,2}$ carries angular momentum $L_z = 2$, we expect that its presence will drive a quench dominated by the spin-2 mode. Indeed, we find that the consequent exact dynamics of $\hat{g}$ behaves according to the description based on spin-2 graviton oscillation [Fig. 8(a)], and is very similar to that obtained by changing the mass tensor in Fig. 3.

Next we consider a quench driven by adding a small amount of $\hat{V}_{0,4}$ component ($c_{0,4} = 0.1$) such that the

interaction changes according to $\hat{V}_0 \to \hat{V}_0 + 0.1\hat{V}_{0,4}$ at $t = 0^+$. This type of quench can be realized in systems whose Fermi contours are not simple ellipses, e.g., where the band dispersion has the form $\epsilon(\mathbf{k}) = k^N \cos(N\theta)$ [89, 90]. As shown in Ref. [90], when $N = 4$, the dominant anisotropic pseudopotential is $V_{0,4}$. Surprisingly, we find $Q(t) \equiv 0$ during the entire measured time interval [see the black solid line in Fig. 8(a)], which suggests that the spin-2 collective mode is not excited. However, the system *does* respond to the perturbation by $\hat{V}_{0,4}$, and we conjecture that this happens by exciting the higher-spin collective modes which cannot be described by the bimetric theory. While we cannot describe the dynamics of higher-spin modes analytically, we can measure the dynamics of quantum fidelity, $|\langle\psi(t)|\psi(0)\rangle|^2$, shown in Fig. 8(b). Clear oscillations in the fidelity are a signature of the non-trivial microscopic dynamics taking place. We note that in the case of $\hat{V}_{0,2}$ quench, fidelity also oscillates, with the same frequency as $\hat{g}$. Moreover, we emphasize that our choice of measuring fidelity was merely a convenience; indeed, observables like entanglement entropy also display quantitatively similar oscillations.

The failure of the bimetric theory to capture the quench dynamics driven by $\hat{V}_{0,4}$ strongly suggests that the $\hat{V}_{0,4}$ quench is dominated by a higher-spin collective mode rather than the spin-2 one. Indeed, unlike the quadrupolar $\hat{V}_{0,2}$, $\hat{V}_{0,4}$ has octupolar structure in momentum space [Fig. 2(b)], which implies that it would couple the ground state to higher-spin excitations. In our case, this is a spin-4 excitation because the odd-spin ones vanish due to inversion symmetry, which is a generic symmetry of LLL-projected FQH Hamiltonians. The spin-4 character of the mode is explicitly confirmed by evaluating the spectral function $\bar{I}_{0,4}(\omega)$ in Fig. 8(c) (with identical results obtained for the discrete Fourier transform, shown in the inset of the same figure). The spectral function shows two peaks, one of which corresponds to the graviton energy and an additional one at higher energy, $\omega \sim 1.7$, which we identify with spin-4 mode. This provides an unambiguous example in which the 2×2 unimodular metric in Eq. (2) is inadequate to capture the dynamics of the Laughlin state, motivating the generalization of the geometrical description of the fractional quantum Hall states and the effective field theory.

VII. CONCLUSIONS AND OUTLOOK

In the present manuscript we have laid out the theoretical foundation for studying the non-equilibrium dynamics of FQH states. We have proposed and numerically simulated the geometric quench protocol which excites neutral collective degrees of freedom of FQH liquids, such as the Laughlin states of bosons at $\nu = 1/2$ and of fermions at $\nu = 1/3$. In all the cases, for the simplest types of quenches which are driven by modifying the mass tensor, we have established that the short-time dynamics after the quench is dominated by the spin-2 graviton mode and accurately agrees with the bimetric theory. Furthermore, we have demonstrated that the geometric quench protocol admits a generalization that allows one to excite higher-spin collective degrees of freedom, whose dynamics cannot be described by the currently available geometric theories of the FQH effect. We believe that the present work will motivate a more detailed study of the geometric degrees of freedom in various strongly correlated systems, and below we highlight several directions that open up for future investigations.

The immediate question which arises is the experimental applicability of our results. Even though the quench protocol can in principle be directly implemented with the available technology, the main challenge is observing coherent dynamics in solid-state materials that currently support FQH states. Assuming typical magnetic fields 10T, we estimate the required time scales for observing the graviton oscillation to be $\sim 10^{-14}$s, which is prohibitively small. The second challenge is how to measure the intrinsic metric in *gapped* FQH states. Recent experiments have successfully measured the anisotropy of the composite fermion Fermi surface induced by tilting the magnetic field [28, 91]. Similar measurements were also performed for hole systems [92]. However, such experiments still need to be generalized to gapped FQH states (we note that acoustic wave absorption has been theoretically proposed as an alternative spectroscopic probe of the graviton [75]). Given the smallness of time scales in solid state FQH materials, a more versatile platform to observe geometric quench could be their analogs in lattice systems – the fractional Chern insulators (FCIs) [93–96]. As we demonstrate in Appendix E, geometric quench that excites a spin-2 mode can be straightforwardly implemented in an FCI, resulting in the same type of dynamics described by the bimetric theory in the long-wavelength limit. Tunability of parameters in FCIs allows to observe time scales on the order of $\sim 10^{-5}$s (assuming the interaction strength in cold-atom settings is in the order of $2\pi\hbar \times 10$kHz), which is well within limits of recent experiments [97].

New dynamical phenomena will likely arise in Abelian FQH states with more complicated internal structure, such as bi-layer states and Jain states. These states host multiple collective modes which would all contribute to the dynamics. Multi-layer systems feature rich phase diagrams that can be explored by tuning the interaction strength between the layers [98, 99]. It would be interesting to map out the dynamical counterparts of such equilibrium phase diagrams by studying the geometric quench in different interaction regimes.

Even in the simplest models of Laughlin states, our study has focused on the linear regime of weak quench. The non-linear regime should become relevant for strong quenches or quenches in the vicinity of the nematic phase transition. The present quench protocol could be used as a complementary tool for probing the nematic transition, which has recently been studied in Ref. [100].

When a "higher-spin" pseudopotential drives the

quench, the system undergoes non-trivial dynamics which cannot be described within the bimetric theory or by anisotropic trial states [101]. In these cases, a richer set of trial states is needed to fully describe the dynamics. This set of states should be parametrized by higher-spin cousins of the intrinsic metric $\hat{g}$. Similar conclusions were reached in Ref. [43] (see also Ref. [102]) where the bimetric theory was argued to be a low-energy approximation to a putative higher-spin theory, and in Ref. [50] where the linearized bimetric for the Jain series at $\nu = n/(2n+1)$ was derived from the Dirac composite Fermi liquid (CFL) theory at large n. In the latter approach the higher-spin modes naturally emerge as collective distortions of the composite Fermi surface. In fact, when the CFL state forms, all of the higher-spin degrees of freedom become gapless, and should be equally important for the dynamics. In these systems, the geometric quench described in the present manuscript, as well as its "higher-spin" cousins, will provide an interesting probe of the collective dynamics of the composite fermion Fermi surface.

The geometric quench also presents an enticing possibility of probing the non-Abelian fractional quantum Hall states, such as the Moore-Read state [8] – a candidate for the observed $\nu = 5/2$ plateau [103]. Numerical works [104, 105] have shown that the Moore-Read state hosts a neutral fermionic mode, in addition to the SMA (bosonic) mode. The neutral fermion mode is expected to have angular momentum 3/2 and is not present in the bimetric theory. It would be very interesting to design the effective theory and numerical probes of this mode at long wavelengths.

Finally, FCIs exhibit much of the same phenomenology as the continuum FQH states (see the recent reviews Refs. [93–95] and references therein). For example, the FCIs also feature the GMP algebra [106, 107], and they naturally correspond to anisotropic FQH states [51, 108]. On the other hand, the FCI states in higher Chern number bands [109–111] do not have usual continuum FQH states as counterparts [112]. Given that the quench driven by anisotropy in hopping has been studied for integer Chern insulators [113, 114], it would be interesting to investigate more systematically the quenches for FCIs, starting from the basic method which we have presented in Appendix E.

VIII. ACKNOWLEDGEMENTS

We thank V. Caudrelier for illuminating discussions about the system of differential equations. This work was supported in part by the Department of Energy, Office of Basic Energy Sciences through Grant No. DE – SC0002140. Z.L. was supported by Alexander von Humboldt Research Fellowship for Postdoctoral Researchers. A.G. was supported by the Leo Kadanoff fellowship, the NSF grant DMR-1206648, and by the University of Chicago Materials Research Science and Engineering Center, which is funded by the National Science Foundation under award No. DMR-1420709. Z.P. acknowledges support by EPSRC grant EP/P009409/1. Statement of compliance with EPSRC policy framework on research data: This publication is theoretical work that does not require supporting research data.

Appendix A: Anisotropic-to-anisotropic quench

As an immediate generalization of the isotropic-to-anisotropic quench studied in Sec. IV A, we now discuss the more general case of a quench with $A_1 > A_0 > 0$, for which the initial state is already anisotropic. In this case, simple analytical solution does not exist under the general initial conditions $Q(0) > 0, \phi(0) = 0$ even for the linearized systems Eqs. (20) and (21). However, by numerically solving the coupled differential equations, we find that the bimetric theory still accurately describes the short-time dynamics of Q and ϕ, and also captures the oscillatory dynamics very well up to moderate times.

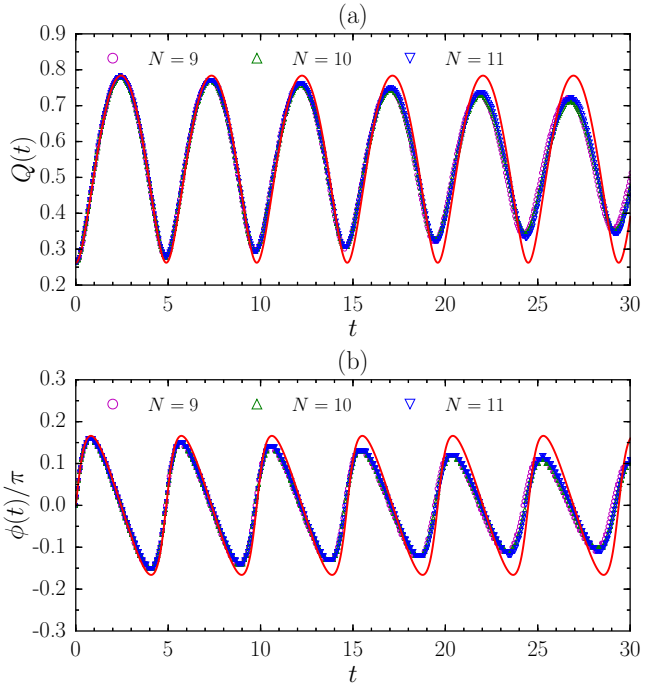

FIG. 9. Exact dynamics of (a) Q and (b) ϕ for $N = 9 - 11$ bosons at $\nu = 1/2$ with the contact interaction. The weak geometric quench is driven by choosing $A_0 = \ln 1.3$ and $A_1 = \ln 1.7$. The red solid curve is the solution of linearized equations Eqs. (20) and (21) under the initial condition $Q(0) = A_0, \phi(0) = 0$, with $A \approx 0.523$ and $E_\gamma \approx 1.283$. These two parameters are obtained by fitting the first oscillation of Q of $N = 11$ against the solution.

In Fig. 9, we choose $A_0 = \ln 1.3$ and $A_1 = \ln 1.7$, and show the exact dynamics for the quench driven by the contact interaction. Since the initial state is a Laughlin model state with $\hat{g}(0) = g_m$, the bimetric theory

predicts the post-quench dynamics of $\hat{g}$ is governed by the solution of Eqs. (20) and (21) with initial condition $Q(0) = A_0, \phi(0) = 0$. Indeed, the numerical data in the first two periods again lie on top of such a solution with fitting parameters $A \approx 0.523$ and $E_\gamma \approx 1.283$. The value of A is close to $A_1 = \ln 1.7 \approx 0.531$, as expected, and $E_\gamma \approx 1.283$ is consistent with the graviton gap estimated from both the $I_{0,2}(\omega)$ spectral function and the previous fit in Fig. 3.

As discussed in Sec. IV A, apart from generally good agreement, we can also observe some discrepancy between the exact dynamics and the equations of the bimetric theory in Fig. 9. This discrepancy is likely caused by the mentioned finite-size effect (the splitting of the spin-2 mode into several states and the Lieb-Robinson light cone) and the possible contribution of higher-spin modes. Compared to isotropic-to-anisotropic quench, stronger finite-size effects in the present case are not surprising because anisotropy effectively reduces the length of the system along one of the spatial directions.

Appendix B: Projected dynamics

In the main text, we have shown that the number of spin-2 eigenstates of H' is exponentially smaller than the full Hilbert space dimension. The number of spin-2 eigenstates was determined by the matrix element of $\hat{V}_{0,2}$ generalized pseudopotential. Here we investigate how accurately the quench dynamics in Sec. IV A can be reproduced by projecting to this set of states.

We perform the projection explicitly, i.e., we calculate the post-quench state as $|\tilde{\psi}(t)\rangle = \frac{1}{\mathcal{N}} \sum_{n\in\mathcal{S}} \exp(-i\epsilon_n t)\langle n|\psi_0\rangle|n\rangle$, where $\mathcal{S}$ contains the first M eigenstates with the largest $|\langle n|\hat{V}_{0,2}|0\rangle|^2$ matrix elements and $\mathcal{N}$ is the normalization factor. The dynamics of the intrinsic metric of $|\tilde{\psi}(t)\rangle$ after an isotropic-anisotropic quench is shown in Fig. 10 for $N = 11$ bosons, together with exact dynamics without the projection. As expected, the projected dynamics approaches the exact dynamics with increasing M. However, for both contact and Coulomb interactions, the main feature in exact dynamics has been accurately reproduced by M less than 10, even if the whole Hilbert space in this case is more than four orders of magnitude larger. Such an excellent approximation of the exact dynamics by a tiny spin-2 fraction of the whole Hilbert space is a compelling evidence for the picture of graviton oscillation and the bimetric theory.

Appendix C: Non-instantaneous quench

Instantaneous quench is the minimal theoretical model that describes sudden tilt of the magnetic field. However, since any experimental manipulation takes finite time, we now generalize our discussions to more realistic, non-instantaneous quenches. To be specific,

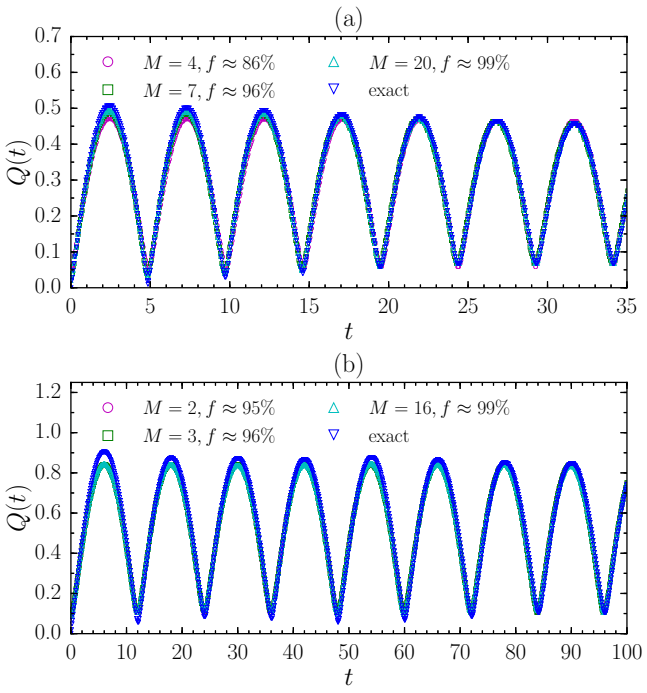

FIG. 10. Dynamics of Q projected to M eigenstates of H' with dominant $|\langle n|\hat{V}_{0,2}|0\rangle|^2$. We consider $N = 11$ bosons at $\nu = 1/2$ with (a) contact and (b) Coulomb interactions. The quench parameters A_0 and A_1 are the same as those in Figs. 3 and 4, respectively.

we consider isotropic-anisotropic quenches driven by a time-dependent ramp of the mass tensor, i.e., $g_m = \mathrm{diag}(e^{A(t)}, e^{-A(t)})$ with

$$A(t) = A_1 \exp(-t_0/t), \tag{C1}$$

such that $A(0) = 0$ and $A(+\infty) = A_1$. The slope of the ramp depends on some characteristic time, t_0. When $t_0 = 0$, we recover the instantaneous quench studied in Sec. IV A. We thus expect that differences between the non-instantaneous quench and the instantaneous one are negligible when t_0 is small, while some qualitative changes may happen for large enough t_0.

As a representative example, we choose $A_1 = \ln 1.3$ (weak quench) and show the predicted behavior of Q and ϕ in the bimetric theory, i.e., the solutions of the full equations [Eqs. (15) and (16)], for different t_0 in Fig. 11. We indeed find that the solutions in the non-instantaneous case agree with their instantaneous limit up to $t_0 \lesssim 10^{-2}$. The effect of the ramp starts to appear when $t_0 \sim 10^{-1}$, which leads to gradual deviations of both the amplitude and frequency in the dynamics from the instantaneous case. Finally, for very large $t_0 \gtrsim 1$, we observe strongly distorted oscillation patterns in Q and ϕ, revealing very different dynamics between the fast-quench and slow-quench regimes.

It would be interesting to compare exact dynamics of finite systems with the predictions of the bimetric theory also for non-instantaneous quenches, as we have

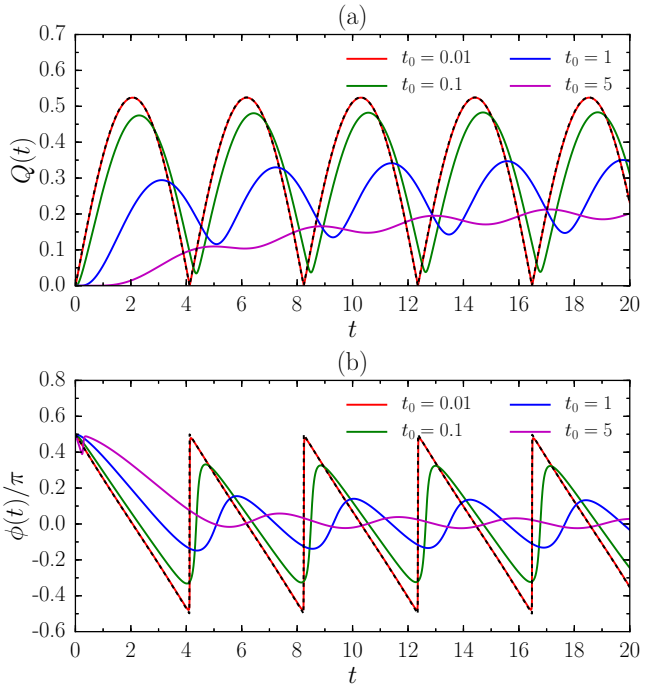

FIG. 11. Solutions of the full equations [Eqs. (15) and (16)] for the non-instantaneous quench with $A(t) = A_1 \exp(-t_0/t)$, under the initial condition $Q(0) = 0$. Here we focus on the $Q \geq 0$ solution. We choose $\Omega = 1.5/4, \gamma = -1, A_1 = \ln 1.3$, and consider several different $t_0 = 0.01$, 0.1, 1 and 5. For comparison, we also give solutions for the instantaneous quench as black dashed lines.

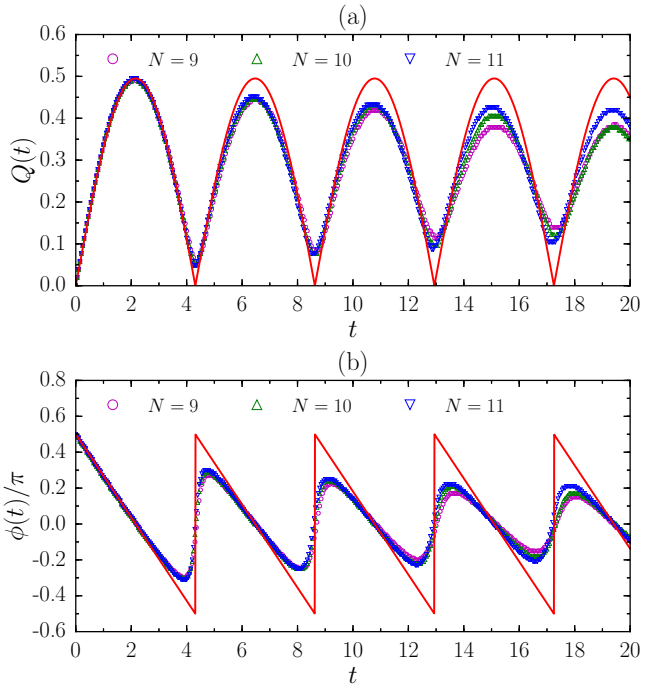

FIG. 12. Exact dynamics of (a) Q and (b) ϕ for $N = 9 - 11$ fermions at $\nu = 1/3$ with the V_1 interaction. The weak geometric quench is driven by choosing $A_0 = 0$ and $A_1 = \ln 1.3$. The red solid curve is the $Q \geq 0$ part of Eqs. (5) and (6), with $A \approx 0.248$ and $E_\gamma \approx 1.457$. These two parameters are obtained by fitting the first oscillation of Q of $N = 11$ against the solution.

done for the instantaneous case in Sec. IV. Due to the time-dependent nature of the non-instantaneous quench, the many-body numerical simulation in this case is more complicated and will be presented in future work. However, because the instantaneous quench corresponds to a stronger perturbation of the system, we expect similar or better agreement between theory and numerics for the case of non-instantaneous quenches.

Appendix D: Weak geometric quench for $\nu = 1/3$ fermions

Here we show the numerical results of the exact dynamics of $\hat{g}$ after a mass anisotropy quench for $\nu = 1/3$ fermions. As representative examples, we focus on weak isotropic-anisotropic quenches with $A_0 = 0$ and $A_1 > 0$, where we choose $A_1 = \ln 1.3$ and $A_1 = \ln 2.0$ for quenches driven by V_1 and Coulomb interactions, respectively. Exact dynamics of $\hat{g}$ up to moderate times is shown in Figs. 12 and 13 for these two types of interactions.

Similar to $\nu = 1/2$ bosons, the short-time dynamics of weak quenches for $\nu = 1/3$ fermions fully agrees with the bimetric theory. We can thus extract parameters A and E_γ by fitting the numerical data against Eqs. (5) and (6), whose values are given in the captions of Figs. 12 and 13. The value of A, which quantifies the anisotropy in the interaction, is again close to A_1 (between 0 and A_1) for the V_1 (Coulomb) interaction as expected. The value of E_γ estimates the graviton gap as 1.46 and 0.14 for V_1 and Coulomb interactions, respectively. Note that the graviton gap of the Coulomb interaction that we extract from the quench dynamics precisely matches the value given by other methods in the context of single-mode approximation [60, 68].

Like in the bosonic case, we also observe deviations from the bimetric theory at longer times for $\nu = 1/3$ fermions. However, these deviations are more serious and appear earlier than those for $\nu = 1/2$ bosons. For quenches driven by the V_1 interaction, while the overall oscillation structure is maintained up to moderate times, the oscillating amplitude already visibly decays after the first oscillation (Fig. 12). The situation is even worse for quenches driven by the Coulomb interaction, as expected. In that case, the behavior of Q and ϕ totally departs from simple oscillations after the first period and the curves of different system sizes are no longer on top of each other (Fig. 13). Compared with $\nu = 1/2$ bosons, our numerical results clearly demonstrate that the dynamics of $\nu = 1/3$ fermions suffers more from finite-size effects in the excitations and the participation of higher-spin modes.

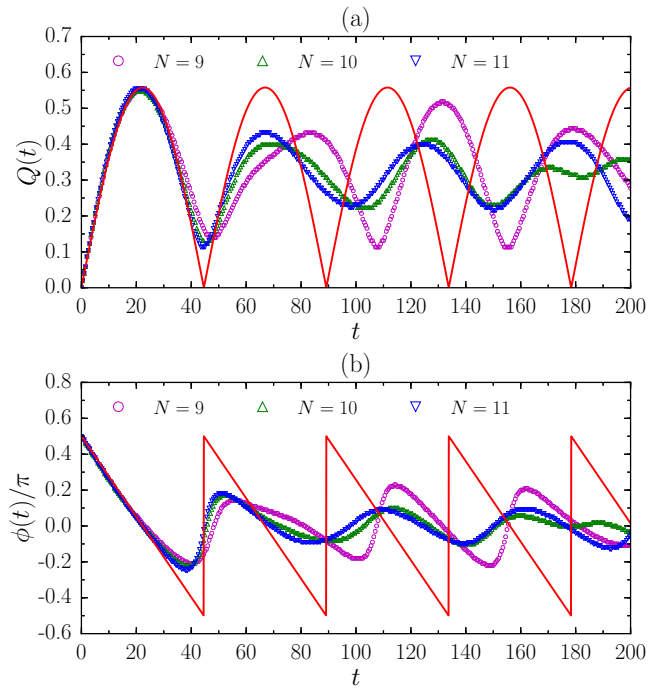

FIG. 13. Exact dynamics of (a) Q and (b) ϕ for $N = 9 - 11$ fermions at $\nu = 1/3$ with the Coulomb interaction. The weak geometric quench is driven by choosing $A_0 = 0$ and $A_1 = \ln 2.0$. The red solid curve is the $Q \geq 0$ part of Eqs. (5) and (6), with $A \approx 0.279$ and $E_\gamma \approx 0.141$. These two parameters are obtained by fitting the first oscillation of Q of $N = 11$ against the solution.

Appendix E: Fractional Chern insulators

Here we generalize the geometric quench from continuum FQH states to their lattice analogs – the fractional Chern insulators (FCIs) [93–95]. Contrary to conventional FQH states, FCIs do not require an external magnetic field [115, 116] and may potentially persist at higher temperatures [117]. Considering the recent experimental progress on quantum many-body dynamics in optical lattices [118], FCIs realized by cold atoms in optical lattices could be a promising platform to observe the dynamics after a geometric quench on much longer time scales than possible in semiconductor FQH systems. In the following, we will describe a quench protocol for FCIs and demonstrate that our main results directly apply to this type of system. As FCIs are inherently anisotropic, the quenches in FCI belong to the anisotropic-anisotropic case discussed in Appendix A.

For concreteness, we consider N bosons in a two-dimensional Ruby lattice [119] of $N_1 \times N_2$ unit cells. The system is in xy plane with periodic boundary conditions. We adopt the same tight-binding parameters and lattice configurations as in Ref. [120], for which the lowest Bloch band is flat and has Chern number $C = 1$. We assume that bosons interact via onsite and dipolar potentials. If all dipoles are polarized in xz plane with an angle α to the $+z$ direction, the interaction Hamiltonian can be written as

$$H_{\rm int} = \sum_i n_i(n_i - 1) + \sum_{i<j} \frac{r_{ij}^2 - 3x_{ij}^2 \sin^2\alpha}{r_{ij}^5} n_i n_j, \tag{E1}$$

where n_i is the occupation on lattice site i, and $r_{ij} = (x_{ij}, y_{ij})$ is the distance between lattice site i and j. We project the interaction to the lowest band and verify that the ground state at band filling $\nu = N/(N_1N_2) = 1/2$ is the $\nu = 1/2$ bosonic Laughlin FCI for a finite range of α, characterized by a robust two-fold topological degeneracy. In order to keep the lattice aspect ratio close to 1 and for the two degenerate FCI states to be located in different momentum sectors, we focus on two system sizes below: $N = 6, N_1 = 3, N_2 = 4$ and $N = 10, N_1 = 4, N_2 = 5$.

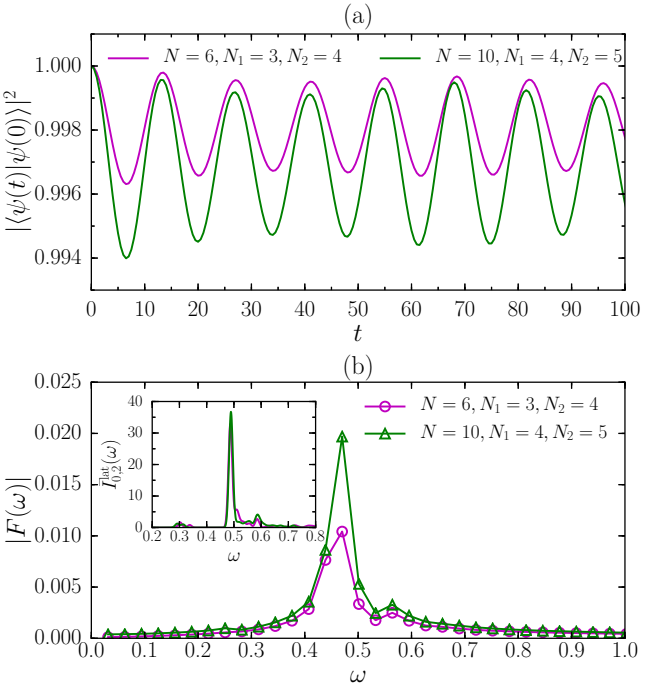

FIG. 14. (a) Dynamics of fidelity, $|\langle\psi(t)|\psi(0)\rangle|^2$, and (b) its discrete Fourier transform for $\nu = 1/2$ bosonic Laughlin FCIs. The weak quench is driven by $\alpha' = 15°$. The inset of (b) shows the normalized spectral function $\bar{I}^{\rm lat}_{0,2}(\omega) = I^{\rm lat}_{0,2}(\omega)/\int I^{\rm lat}_{0,2}(\omega)d\omega$ for the isotropic case with $\alpha = 0$. Markers in insets and curves in main figures with the same color refer to the same system size.

While the interaction is isotropic for $\alpha = 0$, tuning α away from 0 adds anisotropy, which can be experimentally achieved by changing the direction of the polarizing magnetic field [121]. We prepare the initial state as the ground state with momentum $\mathbf{K} = \mathbf{0}$, then drive the quench by suddenly changing α from 0 to a small but finite α' (weak quench). Tuning α is not a direct lattice analogue of changing the geometry of continuum Landau

level orbitals, but it is also expected to excite a geometric degree of freedom in FCIs because it adds quadrupolar anistropy in the system. In order to confirm this, we track the dynamics of fidelity $|\langle\psi(t)|\psi(0)\rangle|^2$, and compare its dominant frequency with the energy of FCI graviton mode which can be probed by a suitable lattice analogue of the $\hat{V}_{0,2}$ pseudopotential. A detailed study of intrinsic metric is also feasible for FCIs by the FCI-FQH mapping [112] and will be presented in a future work.

In Fig. 14, we show the fidelity and its discrete Fourier transform for $\alpha' = 15°$. One can see that the dynamics of fidelity is dominated by a single frequency, characterized by the pronounced peak at $\omega \approx 0.47$ in the discrete Fourier transform [Fig. 14(b)]. In order to estimate the graviton energy on the lattice, we define the operator

$$\hat{V}^{\rm lat}_{0,2} = \sum_{\mathbf{q}} (\cos q_1 - \cos q_2) \bar{\rho}^{\rm lat}_{\mathbf{q}} \bar{\rho}^{\rm lat}_{-\mathbf{q}}, \tag{E2}$$

where $q_i = \mathbf{q}\cdot\mathbf{b}_i$ with $\mathbf{b}_i$'s the two basic lattice direction vectors, $\mathbf{q}$ is in the first Brillouin zone, and $\bar{\rho}^{\rm lat}_{\mathbf{q}}$ is the density operator $e^{i\mathbf{q}\cdot\hat{\mathbf{r}}}$ projected to the lowest Bloch band (see Refs. [69, 112, 122, 123] for the explicit form of $\bar{\rho}^{\rm lat}_{\mathbf{q}}$). Similar to the continuum $\hat{V}_{0,2}$ pseudopotential, $\hat{V}^{\rm lat}_{0,2}$ effectively carries angular momentum $L_z = 2$ to probe spin-2 states on the lattice, because the $\mathbf{q}$-dependence term $\cos q_1 - \cos q_2$ takes a d-wave form $q_1^2 - q_2^2$ at small $|\mathbf{q}|$. Indeed, its spectral function

$$I^{\rm lat}_{0,2}(\omega) = \sum_j \delta(\omega - \epsilon_j) |\langle j|\hat{V}^{\rm lat}_{0,2}|0\rangle|^2 \tag{E3}$$

shows sharply pronounced peaks [inset of Fig. 14(b)], where ϵ_j and $|j\rangle$ are the eigen-energy and eigenstate of the projected interaction Eq. (E1). Since these peaks appear around the same energy as that in the discrete Fourier transform of fidelity, our quench protocol indeed excites the geometric degree of freedom of FCI that corresponds to the spin-2 graviton mode on a lattice. The similarity of the FCI results to the continuum FQH is rather surprising, in light of the fact that there are no quantitative arguments that support the relation between the bimetric theory and FCIs (beyond the intuition mentioned in Ref. [43]).

[1] R. B. Laughlin, "Anomalous quantum hall effect: An incompressible quantum fluid with fractionally charged excitations," Phys. Rev. Lett. **50**, 1395–1398 (1983).
[2] X. G. Wen, "Topological orders in rigid states," Int. J. Mod. Phys. B **04**, 239–271 (1990).
[3] B. I. Halperin, "Quantized hall conductance, current-carrying edge states, and the existence of extended states in a two-dimensional disordered potential," Phys. Rev. B **25**, 2185–2190 (1982).
[4] X.G. Wen, "Edge excitations in the fractional quantum hall states at general filling fractions," Modern Physics Letters B **05**, 39–46 (1991).
[5] R. E. Prange and S. M. Girvin, *The Quantum Hall effect* (Springer-Verlag, 1987).
[6] D. C. Tsui, H. L. Stormer, and A. C. Gossard, "Two-dimensional magnetotransport in the extreme quantum limit," Phys. Rev. Lett. **48**, 1559–1562 (1982).
[7] J. K. Jain, "Composite-fermion approach for the fractional quantum hall effect," Phys. Rev. Lett. **63**, 199–202 (1989).
[8] Gregory Moore and Nicholas Read, "Nonabelions in the fractional quantum hall effect," Nuclear Physics B **360**, 362 – 396 (1991).
[9] N. Read and E. Rezayi, "Beyond paired quantum hall states: Parafermions and incompressible states in the first excited landau level," Phys. Rev. B **59**, 8084–8092 (1999).
[10] S. C. Zhang, T. H. Hansson, and S. Kivelson, "Effective-field-theory model for the fractional quantum hall effect," Phys. Rev. Lett. **62**, 82–85 (1989).
[11] X. G. Wen and A. Zee, "Shift and spin vector: New topological quantum numbers for the hall fluids," Phys. Rev. Lett. **69**, 953–956 (1992).
[12] Andrey Gromov, Gil Young Cho, Yizhi You, Alexander G. Abanov, and Eduardo Fradkin, "Framing anomaly in the effective theory of the fractional quantum hall effect," Phys. Rev. Lett. **114**, 016805 (2015).
[13] J. M. Leinaas and J. Myrheim, "On the theory of identical particles," Nuovo Cimento B Serie **37**, 1–23 (1977).
[14] F. Wilczek, "Quantum Mechanics of Fractional-Spin Particles," Physical Review Letters **49**, 957–959 (1982).
[15] X. G. Wen and A. Zee, "Classification of abelian quantum hall states and matrix formulation of topological fluids," Phys. Rev. B **46**, 2290–2301 (1992).
[16] F. D. M. Haldane and E. H. Rezayi, "Periodic laughlin-jastrow wave functions for the fractional quantized hall effect," Phys. Rev. B **31**, 2529–2531 (1985).
[17] F. D. M. Haldane and E. H. Rezayi, "Finite-size studies of the incompressible state of the fractionally quantized hall effect and its excitations," Phys. Rev. Lett. **54**, 237–240 (1985).
[18] J. K. Jain, *Composite Fermions* (Cambridge University Press, 2007).
[19] Fabian H L Essler and Maurizio Fagotti, "Quench dynamics and relaxation in isolated integrable quantum spin chains," Journal of Statistical Mechanics: Theory and Experiment **2016**, 064002 (2016).
[20] Toshiya Kinoshita, Trevor Wenger, and David S. Weiss, "A quantum newton's cradle," Nature **440**, 900 (2006).
[21] Pasquale Calabrese and John Cardy, "Quantum quenches in 1+1 dimensional conformal field theories," Journal of Statistical Mechanics: Theory and Experiment **2016**, 064003 (2016).
[22] Masahiro Nozaki, Tokiro Numasawa, and Tadashi Takayanagi, "Holographic local quenches and entanglement density," Journal of High Energy Physics **2013**, 80 (2013).
[23] F. Heidrich-Meisner, M. Rigol, A. Muramatsu, A. E. Feiguin, and E. Dagotto, "Ground-state reference systems for expanding correlated fermions in one dimen-

sion," Phys. Rev. A **78**, 013620 (2008).
[24] H. Buljan, R. Pezer, and T. Gasenzer, "Fermi-bose transformation for the time-dependent lieb-liniger gas," Phys. Rev. Lett. **100**, 080406 (2008).
[25] Jorn Mossel, Guillaume Palacios, and Jean-Sébastien Caux, "Geometric quenches in quantum integrable systems," Journal of Statistical Mechanics: Theory and Experiment **2010**, L09001 (2010).
[26] Vincenzo Alba and Fabian Heidrich-Meisner, "Entanglement spreading after a geometric quench in quantum spin chains," Phys. Rev. B **90**, 075144 (2014).
[27] J. P. Eisenstein, R. Willett, H. L. Stormer, D. C. Tsui, A. C. Gossard, and J. H. English, "Collapse of the even-denominator fractional quantum hall effect in tilted fields," Phys. Rev. Lett. **61**, 997–1000 (1988).
[28] D. Kamburov, Yang Liu, M. Shayegan, L. N. Pfeiffer, K. W. West, and K. W. Baldwin, "Composite fermions with tunable fermi contour anisotropy," Phys. Rev. Lett. **110**, 206801 (2013).
[29] J. E. Avron, R. Seiler, and P. G. Zograf, "Viscosity of quantum hall fluids," Phys. Rev. Lett. **75**, 697–700 (1995).
[30] N. Read, "Non-abelian adiabatic statistics and hall viscosity in quantum hall states and $p_x + ip_y$ paired superfluids," Phys. Rev. B **79**, 045308 (2009).
[31] F. D. M. Haldane, ""Hall viscosity" and intrinsic metric of incompressible fractional Hall fluids," ArXiv e-prints (2009), arXiv:0906.1854 [cond-mat.str-el].
[32] J. Maciejko, B. Hsu, S. A. Kivelson, YeJe Park, and S. L. Sondhi, "Field theory of the quantum hall nematic transition," Phys. Rev. B **88**, 125137 (2013).
[33] Yizhi You, Gil Young Cho, and Eduardo Fradkin, "Theory of nematic fractional quantum hall states," Phys. Rev. X **4**, 041050 (2014).
[34] Frank Ferrari and Semyon Klevtsov, "Fqhe on curved backgrounds, free fields and large n," Journal of High Energy Physics **2014**, 86 (2014).
[35] Alexander G. Abanov and Andrey Gromov, "Electromagnetic and gravitational responses of two-dimensional noninteracting electrons in a background magnetic field," Phys. Rev. B **90**, 014435 (2014).
[36] Michael R. Douglas and Semyon Klevtsov, "Bergman kernel from path integral," Communications in Mathematical Physics **293**, 205 (2009).
[37] Barry Bradlyn and N. Read, "Low-energy effective theory in the bulk for transport in a topological phase," Phys. Rev. B **91**, 125303 (2015).
[38] T. Can, M. Laskin, and P. Wiegmann, "Fractional quantum hall effect in a curved space: Gravitational anomaly and electromagnetic response," Phys. Rev. Lett. **113**, 046803 (2014).
[39] S. Klevtsov and P. Wiegmann, "Geometric adiabatic transport in quantum hall states," Phys. Rev. Lett. **115**, 086801 (2015).
[40] Taylor L. Hughes, Robert G. Leigh, and Eduardo Fradkin, "Torsional response and dissipationless viscosity in topological insulators," Phys. Rev. Lett. **107**, 075502 (2011).
[41] Andrey Gromov and Alexander G. Abanov, "Density-curvature response and gravitational anomaly," Phys. Rev. Lett. **113**, 266802 (2014).
[42] F. D. M. Haldane, "Geometrical description of the fractional quantum hall effect," Phys. Rev. Lett. **107**, 116801 (2011).
[43] Andrey Gromov and Dam Thanh Son, "Bimetric theory of fractional quantum hall states," Phys. Rev. X **7**, 041032 (2017).
[44] P. Wiegmann, "Inner nonlinear waves and inelastic light scattering of fractional quantum hall states as evidence of the gravitational anomaly," Phys. Rev. Lett. **120**, 086601 (2018).
[45] F. D. M. Haldane, "Self-duality and long-wavelength behavior of the Landau-level guiding-center structure function, and the shear modulus of fractional quantum Hall fluids," ArXiv e-prints (2011), arXiv:1112.0990 [cond-mat.str-el].
[46] Bo Yang, Zi-Xiang Hu, Z. Papić, and F. D. M. Haldane, "Model wave functions for the collective modes and the magnetoroton theory of the fractional quantum hall effect," Phys. Rev. Lett. **108**, 256807 (2012).
[47] Siavash Golkar, Dung X. Nguyen, and Dam T. Son, "Spectral sum rules and magneto-roton as emergent graviton in fractional quantum hall effect," Journal of High Energy Physics **2016**, 21 (2016).
[48] Eric A. Bergshoeff, Sjoerd de Haan, Olaf Hohm, Wout Merbis, and Paul K. Townsend, "Zwei-dreibein gravity: A two-frame-field model of 3d massive gravity," Phys. Rev. Lett. **111**, 111102 (2013).
[49] Eric A Bergshoeff, Jan Rosseel, and Paul K Townsend, "Gravity and the spin-2 planar schroedinger equation," Physical review letters **120**, 141601 (2018).
[50] D. X. Nguyen, A. Gromov, and D. Thanh Son, "Fractional quantum Hall systems near nematicity: bimetric theory, composite fermions, and Dirac brackets," ArXiv e-prints (2017), arXiv:1712.08169 [cond-mat.str-el].
[51] Bo Yang, Zi-Xiang Hu, Ching Hua Lee, and Z. Papić, "Generalized pseudopotentials for the anisotropic fractional quantum hall effect," Phys. Rev. Lett. **118**, 146403 (2017).
[52] Avinash Dhar, Gautam Mandal, and Spenta R Wadia, "Non-relativistic fermions, coadjoint orbits of w and string field theory at c= 1," Modern Physics Letters A **7**, 3129–3145 (1992).
[53] A Jevicki and B Sakita, "The quantum collective field method and its application to the planar limit," in *The Large N Expansion In Quantum Field Theory And Statistical Physics: From Spin Systems to 2-Dimensional Gravity* (World Scientific, 1993) pp. 402–418.
[54] Simone Giombi, Igor R Klebanov, and Arkady A Tseytlin, "Partition functions and casimir energies in higher spin ads d+ 1/cft d," Physical Review D **90**, 024048 (2014).
[55] Gerald A Goldin, Ralph Menikoff, and David H Sharp, "Diffeomorphism groups and quantized vortex filaments," Physical review letters **58**, 2162 (1987).
[56] Vladimir I Arnold and Boris A Khesin, "Topological methods in hydrodynamics," Annual review of fluid mechanics **24**, 145–166 (1992).
[57] Itzhak Bars, "Strings from reduced large-n gauge theory via area preserving diffeomorphisms," Physics Letters B **245**, 35–42 (1990).
[58] N. R. Cooper, N. K. Wilkin, and J. M. F. Gunn, "Quantum phases of vortices in rotating bose-einstein condensates," Phys. Rev. Lett. **87**, 120405 (2001).
[59] N. Regnault and Th. Jolicoeur, "Quantum hall fractions in rotating bose-einstein condensates," Phys. Rev. Lett. **91**, 030402 (2003).
[60] S. M. Girvin, A. H. MacDonald, and P. M. Platz-

man, "Collective-excitation gap in the fractional quantum hall effect," Phys. Rev. Lett. **54**, 581–583 (1985).
[61] Bo Yang, Z. Papić, E. H. Rezayi, R. N. Bhatt, and F. D. M. Haldane, "Band mass anisotropy and the intrinsic metric of fractional quantum hall systems," Phys. Rev. B **85**, 165318 (2012).
[62] Hao Wang, Rajesh Narayanan, Xin Wan, and Fuchun Zhang, "Fractional quantum hall states in two-dimensional electron systems with anisotropic interactions," Phys. Rev. B **86**, 035122 (2012).
[63] T. Gokmen, Medini Padmanabhan, and M. Shayegan, "Transference of transport anisotropy to composite fermions," Nature Physics **6**, 621 EP – (2010).
[64] Z. Papić, "Fractional quantum hall effect in a tilted magnetic field," Phys. Rev. B **87**, 245315 (2013).
[65] Bo Yang, Ching Hua Lee, Chi Zhang, and Zi-Xiang Hu, "Anisotropic pseudopotential characterization of quantum hall systems under a tilted magnetic field," Phys. Rev. B **96**, 195140 (2017).
[66] Sonika Johri, Z Papić, P Schmitteckert, R N Bhatt, and F D M Haldane, "Probing the geometry of the laughlin state," New Journal of Physics **18**, 025011 (2016).
[67] F Duncan M Haldane, "Fractional quantization of the hall effect-a hierarchy of incompressible quantum fluid states," Physical Review Letters **51**, 605–608 (1983).
[68] S. M. Girvin, A. H. MacDonald, and P. M. Platzman, "Magneto-roton theory of collective excitations in the fractional quantum hall effect," Phys. Rev. B **33**, 2481–2494 (1986).
[69] Cécile Repellin, Titus Neupert, Zlatko Papić, and Nicolas Regnault, "Single-mode approximation for fractional chern insulators and the fractional quantum hall effect on the torus," Phys. Rev. B **90**, 045114 (2014).
[70] Bo Yang, Zi-Xiang Hu, Z. Papić, and F. D. M. Haldane, "Model wave functions for the collective modes and the magnetoroton theory of the fractional quantum hall effect," Phys. Rev. Lett. **108**, 256807 (2012).
[71] Thierry Jolicoeur, "Shape of the magnetoroton at $\nu = 1/3$ and $\nu = 7/3$ in real samples," Phys. Rev. B **95**, 075201 (2017).
[72] F. D. M. Haldane, "Many-particle translational symmetries of two-dimensional electrons at rational landau-level filling," Phys. Rev. Lett. **55**, 2095–2098 (1985).
[73] F. D. M. Haldane, "Fractional quantization of the hall effect: A hierarchy of incompressible quantum fluid states," Phys. Rev. Lett. **51**, 605–608 (1983).
[74] Andrey Gromov, Scott D. Geraedts, and Barry Bradlyn, "Investigating anisotropic quantum hall states with bimetric geometry," Phys. Rev. Lett. **119**, 146602 (2017).
[75] Kun Yang, "Acoustic wave absorption as a probe of dynamical geometrical response of fractional quantum hall liquids," Phys. Rev. B **93**, 161302 (2016).
[76] Sean M Carroll, *Spacetime and geometry. An introduction to general relativity* (2004).
[77] Fabio Franchini, Andrey Gromov, Manas Kulkarni, and Andrea Trombettoni, "Universal dynamics of a soliton after an interaction quench," Journal of Physics A: Mathematical and Theoretical **48**, 28FT01 (2015).
[78] Elliott H. Lieb and Derek W. Robinson, "The finite group velocity of quantum spin systems," Comm. Math. Phys. **28**, 251–257 (1972).
[79] Andrea Cappelli, Carlo A Trugenberger, and Guillermo R Zemba, "Infinite symmetry in the quantum hall effect," Nuclear Physics B **396**, 465–490 (1993).
[80] Andrea Cappelli and Enrico Randellini, "Multipole expansion in the quantum hall effect," Journal of High Energy Physics **2016**, 105 (2016).
[81] Siavash Golkar, Dung Xuan Nguyen, Matthew M Roberts, and Dam Thanh Son, "Higher-spin theory of the magnetorotons," Physical review letters **117**, 216403 (2016).
[82] MP Blencowe, "A consistent interacting massless higher-spin field theory in d= 2+ 1," Classical and Quantum Gravity **6**, 443 (1989).
[83] E Bergshoeff, MP Blencowe, and Kellogg S Stelle, "Area-preserving diffeomorphisms and higher-spin algebras," Communications in Mathematical Physics **128**, 213–230 (1990).
[84] Leonard Susskind, "The quantum hall fluid and non-commutative chern simons theory," arXiv preprint hep-th/0101029 (2001).
[85] Alexios P Polychronakos, "Quantum hall states as matrix chern-simons theory," Journal of High Energy Physics **2001**, 011 (2001).
[86] Simeon Hellerman and Mark Van Raamsdonk, "Quantum hall physics= noncommutative field theory," Journal of High Energy Physics **2001**, 039 (2001).
[87] Satoshi Iso, Dimitra Karabali, and Bunji Sakita, "Fermions in the lowest landau level. bosonization, w algebra, droplets, chiral bosons," Physics Letters B **296**, 143–150 (1992).
[88] N Read, "Lowest-landau-level theory of the quantum hall effect: The fermi-liquid-like state of bosons at filling factor one," Physical Review B **58**, 16262 (1998).
[89] F. D. M. Haldane and Y. Shen, "Geometry of Landau orbits in the absence of rotational symmetry," ArXiv e-prints (2015), arXiv:1512.04502 [cond-mat.mes-hall].
[90] Matteo Ippoliti, Scott D. Geraedts, and R. N. Bhatt, "Composite fermions in bands with n-fold rotational symmetry," Phys. Rev. B **96**, 115151 (2017).
[91] D. Kamburov, M. A. Mueed, M. Shayegan, L. N. Pfeiffer, K. W. West, K. W. Baldwin, J. J. D. Lee, and R. Winkler, "Fermi contour anisotropy of gaas electron-flux composite fermions in parallel magnetic fields," Phys. Rev. B **89**, 085304 (2014).
[92] M. A. Mueed, D. Kamburov, Yang Liu, M. Shayegan, L. N. Pfeiffer, K. W. West, K. W. Baldwin, and R. Winkler, "Composite fermions with a warped fermi contour," Phys. Rev. Lett. **114**, 176805 (2015).
[93] Siddharth A. Parameswaran, Rahul Roy, and Shivaji L. Sondhi, "Fractional quantum hall physics in topological flat bands," Comptes Rendus Physique **14**, 816 – 839 (2013).
[94] Emil J. Bergholtz and Zhao Liu, "Topological flat band models and fractional chern insulators," International Journal of Modern Physics B **27**, 1330017 (2013).
[95] Titus Neupert, Claudio Chamon, Thomas Iadecola, Luiz H Santos, and Christopher Mudry, "Fractional (chern and topological) insulators," Physica Scripta **2015**, 014005 (2015).
[96] Eric M. Spanton, Alexander A. Zibrov, Haoxin Zhou, Takashi Taniguchi, Kenji Watanabe, Michael P. Zaletel, and Andrea F. Young, "Observation of fractional chern insulators in a van der waals heterostructure," Science **360**, 62–66 (2018).
[97] Hannes Bernien, Sylvain Schwartz, Alexander Keesling, Harry Levine, Ahmed Omran, Hannes Pichler, Soon-

won Choi, Alexander S. Zibrov, Manuel Endres, Markus Greiner, Vladan Vuletic, and Mikhail D. Lukin, "Probing many-body dynamics on a 51-atom quantum simulator," Nature **551**, 579 EP – (2017), article.

[98] "Multicomponent quantum hall systems: The sum of their parts and more," in *Perspectives in Quantum Hall Effects* (Wiley-VCH Verlag GmbH, 2007) pp. 161–224.

[99] J.P. Eisenstein, "Exciton condensation in bilayer quantum hall systems," Annual Review of Condensed Matter Physics **5**, 159–181 (2014).

[100] N. Regnault, J. Maciejko, S. A. Kivelson, and S. L. Sondhi, "Evidence of a fractional quantum hall nematic phase in a microscopic model," Phys. Rev. B **96**, 035150 (2017).

[101] R.-Z. Qiu, F. D. M. Haldane, Xin Wan, Kun Yang, and Su Yi, "Model anisotropic quantum hall states," Phys. Rev. B **85**, 115308 (2012).

[102] Andrea Cappelli and Enrico Randellini, "Multipole expansion in the quantum hall effect," Journal of High Energy Physics **2016**, 105 (2016).

[103] R. Willett, J. P. Eisenstein, H. L. Störmer, D. C. Tsui, A. C. Gossard, and J. H. English, "Observation of an even-denominator quantum number in the fractional quantum hall effect," Phys. Rev. Lett. **59**, 1776–1779 (1987).

[104] Parsa Bonderson, Adrian E. Feiguin, and Chetan Nayak, "Numerical calculation of the neutral fermion gap at the $\nu = 5/2$ fractional quantum hall state," Phys. Rev. Lett. **106**, 186802 (2011).

[105] Gunnar Möller, Arkadiusz Wójs, and Nigel R. Cooper, "Neutral fermion excitations in the moore-read state at filling factor $\nu = 5/2$," Phys. Rev. Lett. **107**, 036803 (2011).

[106] Thomas Scaffidi and Steven H. Simon, "Exact solutions of fractional chern insulators: Interacting particles in the hofstadter model at finite size," Phys. Rev. B **90**, 115132 (2014).

[107] Rahul Roy, "Band geometry of fractional topological insulators," Phys. Rev. B **90**, 165139 (2014).

[108] Fenner Harper, Steven H. Simon, and Rahul Roy, "Perturbative approach to flat chern bands in the hofstadter model," Phys. Rev. B **90**, 075104 (2014).

[109] Zhao Liu, Emil J. Bergholtz, Heng Fan, and Andreas M. Läuchli, "Fractional chern insulators in topological flat bands with higher chern number," Phys. Rev. Lett. **109**, 186805 (2012).

[110] Yi-Fei Wang, Hong Yao, Chang-De Gong, and D. N. Sheng, "Fractional quantum hall effect in topological flat bands with chern number two," Phys. Rev. B **86**, 201101 (2012).

[111] A. Sterdyniak, C. Repellin, B. Andrei Bernevig, and N. Regnault, "Series of abelian and non-abelian states in $c > 1$ fractional chern insulators," Phys. Rev. B **87**, 205137 (2013).

[112] Yang-Le Wu, N. Regnault, and B. Andrei Bernevig, "Bloch model wave functions and pseudopotentials for all fractional chern insulators," Phys. Rev. Lett. **110**, 106802 (2013).

[113] Matthew Killi and Arun Paramekanti, "Use of quantum quenches to probe the equilibrium current patterns of ultracold atoms in an optical lattice," Phys. Rev. A **85**, 061606 (2012).

[114] Matthew Killi, Stefan Trotzky, and Arun Paramekanti, "Anisotropic quantum quench in the presence of frustration or background gauge fields: A probe of bulk currents and topological chiral edge modes," Phys. Rev. A **86**, 063632 (2012).

[115] Kai Sun, Zhengcheng Gu, Hosho Katsura, and S. Das Sarma, "Nearly flatbands with nontrivial topology," Phys. Rev. Lett. **106**, 236803 (2011).

[116] Titus Neupert, Luiz Santos, Claudio Chamon, and Christopher Mudry, "Fractional quantum hall states at zero magnetic field," Phys. Rev. Lett. **106**, 236804 (2011).

[117] Evelyn Tang, Jia-Wei Mei, and Xiao-Gang Wen, "High-temperature fractional quantum hall states," Phys. Rev. Lett. **106**, 236802 (2011).

[118] Tim Langen, Remi Geiger, and Jörg Schmiedmayer, "Ultracold atoms out of equilibrium," Annual Review of Condensed Matter Physics **6**, 201–217 (2015).

[119] Xiang Hu, Mehdi Kargarian, and Gregory A. Fiete, "Topological insulators and fractional quantum hall effect on the ruby lattice," Phys. Rev. B **84**, 155116 (2011).

[120] Yang-Le Wu, B. Andrei Bernevig, and N. Regnault, "Zoology of fractional chern insulators," Phys. Rev. B **85**, 075116 (2012).

[121] S. Baier, M. J. Mark, D. Petter, K. Aikawa, L. Chomaz, Z. Cai, M. Baranov, P. Zoller, and F. Ferlaino, "Extended bose-hubbard models with ultracold magnetic atoms," Science **352**, 201–205 (2016).

[122] S. A. Parameswaran, R. Roy, and S. L. Sondhi, "Fractional chern insulators and the W_∞ algebra," Phys. Rev. B **85**, 241308 (2012).

[123] B. Andrei Bernevig and N. Regnault, "Emergent many-body translational symmetries of abelian and non-abelian fractionally filled topological insulators," Phys. Rev. B **85**, 075128 (2012).